

2

AD-A258 716



PL-TR-92-2209

SIMULATION AND CALCULATION OF THE APEX ATTITUDE

W. J. McNeil

DTIC
S **ELECTE** **D**
NOV 12 1992
C

Radex, Inc.
Three Preston Court
Bedford, MA 01730

29 July 1992

Scientific Report No. 11


Approved for public release; distribution unlimited

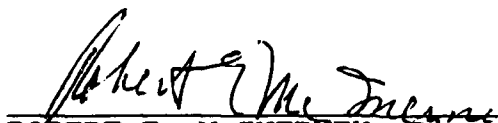
92-29309



PHILLIPS LABORATORY
Directorate of Geophysics
AIR FORCE MATERIEL COMMAND
HANSCOM AIR FORCE BASE, MA 01731-5000

"This technical report has been reviewed and is approved for publication"


EDWARD C. ROBINSON
Contract Manager
Data Analysis Division


ROBERT E. MCINERNEY, Director
Data Analysis Division

This report has been reviewed by the ESD Public Affairs Office (PA) and is releasable to the National Technical Information Service (NTIS).

Qualified requestors may obtain additional copies from the Defense Technical Information Center. All others should apply to the National Technical Information Service.

If your address has changed, or if you wish to be removed from the mailing list, or if the addressee is no longer employed by your organization, please notify GL/IMA, Hanscom AFB, MA 01731. This will assist us in maintaining a current mailing list.

Do not return copies of this report unless contractual obligations or notices on a specific document requires that it be returned.

REPORT DOCUMENTATION PAGE			Form Approved OMB No. 0704-0188	
<small>Public reporting burden for this collection of information is estimated to average 1 hour per response, including the time for reviewing instructions, searching existing data sources, gathering and maintaining the data needed, and completing and reviewing the collection of information. Send comments regarding this burden estimate or any other aspect of this collection of information, including suggestions for reducing this burden, to Washington Headquarters Services, Directorate for Information Operations and Reports, 1215 Jefferson Davis Highway, Suite 1204 Arlington, VA 22202-4302, and to the Office of Management and Budget, Paperwork Reduction Project (0704-0188), Washington, DC 20503.</small>				
1. AGENCY USE ONLY (Leave blank)	2. REPORT DATE 29 July 1992	3. REPORT TYPE AND DATES COVERED Scientific Report No. 11		
4. TITLE AND SUBTITLE Simulation and Calculation of the APEX Attitude		5. FUNDING NUMBERS PE 62101F PR 7659 TA 05 WU AB Contract F19628-89-C-0068		
6. AUTHOR(S) W. J. McNeil				
7. PERFORMING ORGANIZATION NAME(S) AND ADDRESS(ES) RADEX, Inc. Three Preston Court Bedford, MA 01730		8. PERFORMING ORGANIZATION REPORT NUMBER RXR-92072		
9. SPONSORING / MONITORING AGENCY NAME(S) AND ADDRESS(ES) Phillips Laboratory Hanscom AFB, MA 01731-5000 Contract Manager: Edward C. Robinson/GPD		10. SPONSORING / MONITORING AGENCY REPORT NUMBER PL-TR-92-2209		
11. SUPPLEMENTARY NOTES				
12a. DISTRIBUTION / AVAILABILITY STATEMENT Approved for Public Release Distribution Unlimited		12b. DISTRIBUTION CODE		
13. ABSTRACT (Maximum 200 words) <p>A simulation of the APEX attitude is carried out for purposes of development and testing of attitude computation algorithms and for assessment of the accuracy of post-flight attitude determination. It is found that reasonably tractable algorithms give adequate accuracy for determination of attitude control in the vehicle. Sun normal angle will be known to a high precision during sunlit operations. The roll axis in sunlight and the three axes during eclipse will be somewhat less precise, depending mainly on the degree of magnetic contamination. However, it is estimated that these quantities will be of sufficient accuracy as well.</p>				
14. SUBJECT TERMS Attitude simulation, Attitude determination, APEX attitude			15. NUMBER OF PAGES 54	
			16. PRICE CODE	
17. SECURITY CLASSIFICATION OF REPORT Unclassified	18. SECURITY CLASSIFICATION OF THIS PAGE Unclassified	19. SECURITY CLASSIFICATION OF ABSTRACT Unclassified	20. LIMITATION OF ABSTRACT Unlimited	

TABLE OF CONTENTS

<u>Section</u>	<u>Page</u>
1.0 INTRODUCTION	1
2.0 DEFINITION OF THE ATTITUDE	2
2.1 CONVERSION TO INERTIAL COORDINATES	2
2.2 CONVERSION FROM INERTIAL COORDINATES	6
3.0 MODELING THE ATTITUDE	7
3.1 EPHEMERIS MODELING	7
3.2 MODELING ENVIRONMENTAL TORQUES	8
3.3 MODELING CONTROL LAWS	9
3.4 INCLUDING MAGNETOMETER EFFECTS	12
3.5 ECLIPSE CONTROL LAWS	13
3.6 EQUATIONS OF MOTION	13
3.7 SIMULATION RESULTS	14
3.8 SIMULATION OF INSTRUMENTS	21
4.0 ATTITUDE SOLUTION ALGORITHMS	22
4.1 MAGNETOMETER CALIBRATION	22
4.2 ATTITUDE SOLUTIONS IN SUNLIGHT	23
4.3 ATTITUDE SOLUTIONS IN ECLIPSE	32
5.0 EVALUATION OF ON-BOARD ATTITUDE	41
6.0 CONCLUSION	43
REFERENCES	45
APPENDIX. STATE VECTORS	A-1

DISC QUALITY INSPECTED

Accession For	
NIIS	<input checked="" type="checkbox"/>
DTIC TAB	<input type="checkbox"/>
Unannounced	<input type="checkbox"/>
Justification	
By	
Distribution/	
Availability Codes	
Avail and/or	
Dist	Special
A-1	

LIST OF FIGURES

<u>Figure</u>	<u>Page</u>
1. Pitch, yaw and roll angles defining the APEX Attitude	3
2. Two possible configurations satisfying the nominal attitude requirements	4
3. Typical aerodynamic and gravity gradient torques for APEX	10
4. Typical pitch and yaw angles during sunlit operation	15
5. Values of roll axis attitude with low and high frequency induced fields	16
6. Roll axis attitude with various static induced fields	18
7. Torque rod commands	19
8. Pitch and yaw angles for orbits with eclipses	20
9. Results of magnetometer calibration with $B_i=200$ and $B_r=120$ nT	24
10. Same as Figure 9 but with $B_i=500$ nT	25
11. Pitch and yaw angles calculated during sunlit operation	27
12. Roll axis, actual and calculated with and without calibration	29
13. Calibrated roll error in sunlight	30
14. Errors in roll arising from timing & ephemeris errors	31
15. Pitch, yaw and roll during eclipse	33
16. Best fit solution with constant attitude for data in Figure 15	36
17. Attitude and solution for Eclipse 2 of Case 10	37
18. Attitude and solution for a non-nominal case	39
19. Attitude and constant solution for no control during eclipse	40
20. Same as Figure 19 but with linear term in ϕ	42
21. Case 9 Eclipse 2 solution with fixed derivatives	44

LIST OF TABLES

<u>Table</u>	<u>Page</u>
1. Control Law Coefficients	11

ACKNOWLEDGEMENTS

We greatly appreciate the efforts of Al Griffin, PL/GPD, Dennis Delorey, Boston College, who have assisted in the ground work necessary for the understanding of the attitude requirements of this mission and of the specifics of the attitude instruments. Rick Barnison, of Orbital Sciences Corp., has been most helpful in regards to the attitude control system and the instruments. The orbit propagator used to generate test elements was provided by Johnny Kwok of JPL.

1.0 INTRODUCTION

In the design, development and testing of attitude determination and processing algorithms, it is necessary to perform at least a rudimentary simulation of the satellite orbit and data from the attitude instruments. This is especially true for actively controlled satellites, since the attitude characteristics depend on the interplay between the environmental torques and control mechanisms of the satellite. In order to assess the feasibility of computational techniques, realistic data must be generated. Simulation is also necessary for the generation of software test data and it is valuable in that it gives one a sense of the type of behavior to expect, although perhaps not in a truly precise manner, before launch. This often dramatically decreases the start-up time for data processing. This report details the modeling carried out for the Advanced Photovoltaic and Electronic Experiment (APEX) satellite (P90-1). It describes the algorithms selected for the post-flight Orbital Data Processing System for calibration of the magnetometer and for attitude computation. As a by-product, several interesting features that may be present in the APEX attitude behavior are noted.

The APEX satellite supports three experiments; the Photovoltaic Array Space Power Plus Diagnostics (PASP-Plus) experiment, the Cosmic Ray Upset Experiment/Cosmic Ray Environment and Dosimeter Experiment (CRUX/CREDO), and the Ferroelectric Memory Experiment (FERRO). Attitude control requirements are strictest during sunlit operation, when the sun must be normal to the solar arrays to within one-half degree. This requires the spacecraft x-axis to be collinear with the sun direction to this precision. A second, less precise requirement is that the dosimeter (spacecraft y-axis) lie in the ecliptic plane to within 5° . There are no set requirements for attitude knowledge, however, knowledge must be sufficient to assess the level of control. For the APEX satellite, assessment of the degree of attitude control is the primary purpose of post-flight attitude computation.

The attitude determination instruments aboard the satellite consist of a two-axis sun sensor, which measures the sun normal vector directly, and a magnetometer, which can be used to calculate the roll angle during sunlit operation and three-axis attitude in eclipse. Knowledge of the x-axis relative to the sun is thus readily available when the solar panels are illuminated. The secondary requirement for roll axis attitude in sunlight and three-axis attitude in eclipse must be evaluated from magnetometer data alone. Such calculations are unvaryingly quite sensitive to calibration errors and to spacecraft induced fields, so that calibration of the instrument and evaluation of the spacecraft cleanliness become synonymous with attitude determination.

The purpose of this work is to investigate the dynamics of the satellite under 'nominal' conditions, to define and assess algorithms for calibration of the magnetometer and for attitude calculation and ultimately to demonstrate that attitude can be calculated with sufficient accuracy for determination of the degree of attitude control. It is not the subject of this work to determine whether such control will be possible in flight, however, we would like to be reasonably sure that the attitude is calculated properly should non-nominal situations arise. In the next section, the attitude is defined. Following this, we discuss the modeling of the APEX ephemeris, environmental torques and control laws. Finally, we demonstrate the algorithms chosen for

magnetometer calibration and for attitude calculation. In the course of this work, we are able to arrive at some rough estimates for the accuracy of the calculated attitude.

2.0 DEFINITION OF THE ATTITUDE

Generally speaking, it is possible to define the spacecraft attitude in several ways, so long as the process of computation and utilization of the attitude solution are based on the same definition. However, because the APEX data stream contains an on-board attitude solution as well as raw sensor data, it is necessary to adopt the same definition for post-flight determination as is used in the on-board solution.

The APEX attitude is defined by three angles, the values of which are simultaneously zero when the spacecraft is in its nominal attitude. This nominal attitude consists of the spacecraft x-axis pointed directly toward the sun and the spacecraft y-axis resting in the earth's ecliptic plane. These three angles are further defined by rotations about the three spacecraft axes. These angles will be called θ_x , θ_y and θ_z in what follows. Figure 1 shows these angles and their relationship to the defining sun and ecliptic vectors. All three of these angles are defined as the rotation which the spacecraft has undergone *away* from its nominal position. This means that, when the sun is in the quadrant shown in Figure 1, θ_z is negative and θ_y is positive. (Positive rotations are taken to be clockwise looking *along* the axis of rotation.) Thus, θ_z is the negative of the first measurement of the sun sensor and θ_y is equal to the second sun sensor measurement. θ_y and θ_z are called pitch and yaw respectively by the designers of the APEX Attitude Determination and Control System.

The roll axis is defined with the same sense as well, if the spacecraft y-axis has rotated in a clockwise manner from the ecliptic plane with respect to the x-axis, the angle is positive. There is an ambiguity in the definition, however, depending on whether the spacecraft y-axis points toward or away from the earth as the satellite moves toward the sun. These two cases are shown schematically in Figure 2. If the satellite is in configuration 1 and the y-axis is above the plane, a negative rotation about the x-axis has taken place. If in configuration 2 and above the plane, the rotation was positive. We will allow for both these cases in what follows. The configuration can be easily deduced from the sign of the z-axis magnetic field. θ_x is known as roll in the APEX system.

2.1 CONVERSION TO INERTIAL COORDINATES

In order to perform attitude simulation and determination, it is necessary to transform between the 'natural' system of θ_x , θ_y and θ_z , or equivalently, pitch, roll and yaw, and an inertial frame in which the directions of geophysical vectors and the spacecraft position are defined. One convenient frame is Earth Centered Inertial (ECI) coordinates. In this system, the z-axis is coincident with the Earth's rotation axis and the x-axis points toward the vernal equinox in the ecliptic plane. We transform pitch, roll and yaw to ECI as follows:

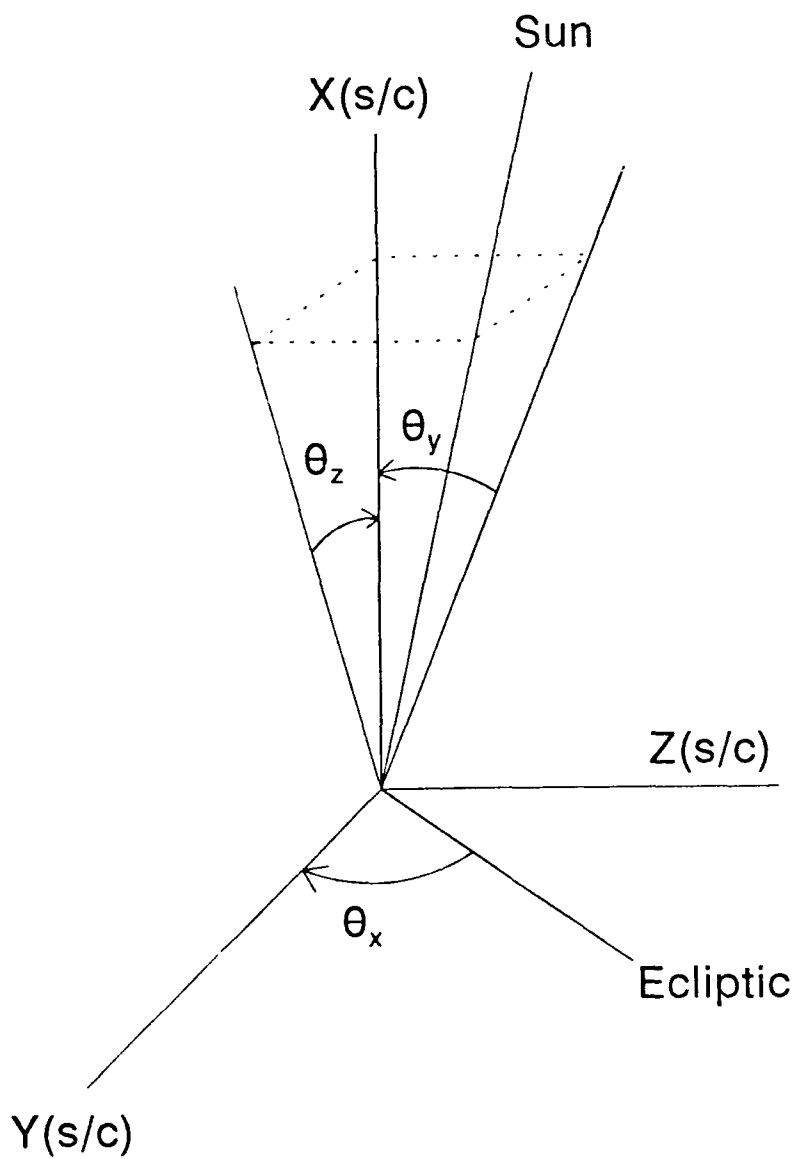


Figure 1. Pitch, yaw and roll angles defining the APEX attitude. In this example, the sun vector is above the plane of the paper and the spacecraft axes have moved by θ_x , θ_y and θ_z .

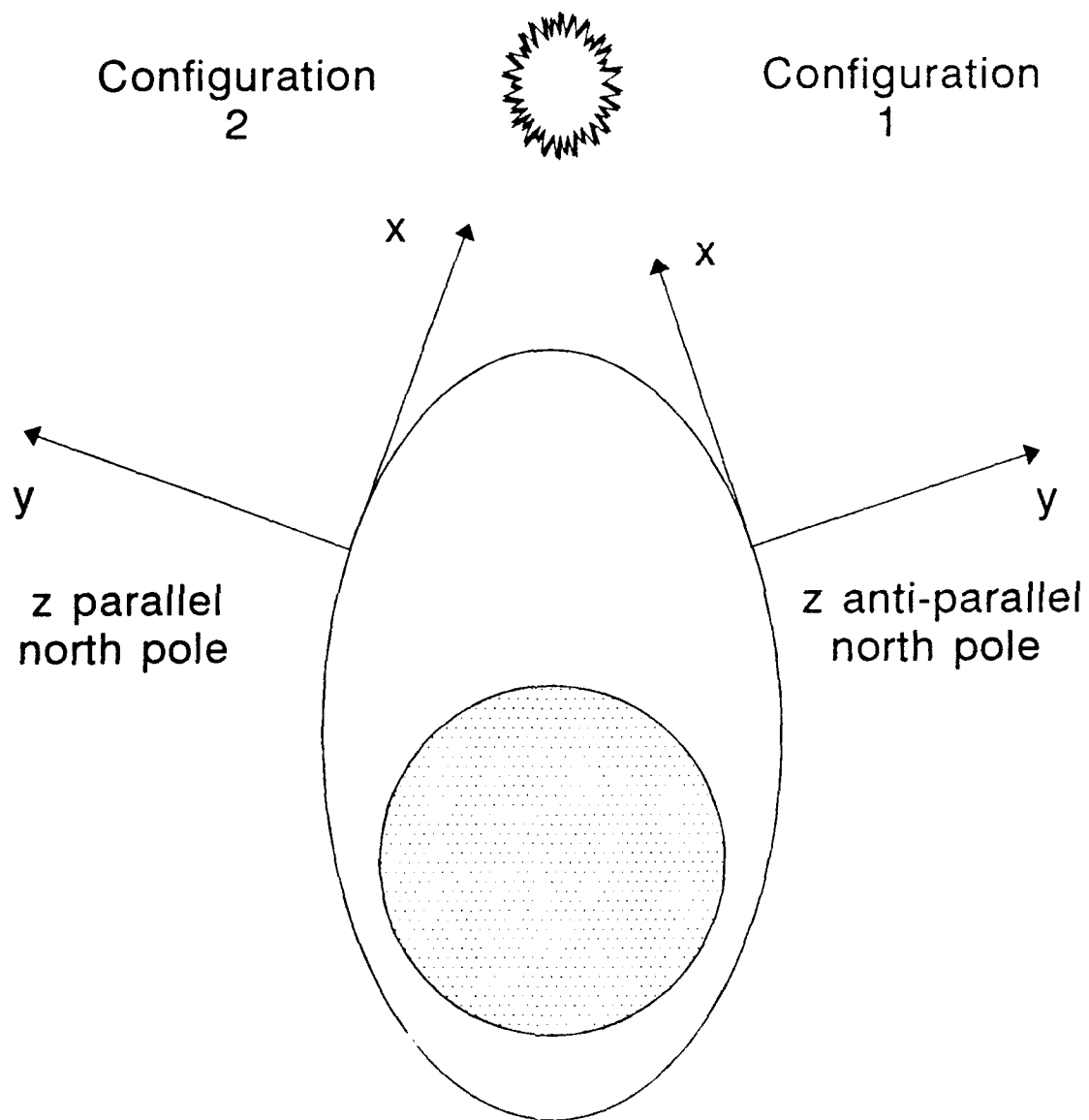


Figure 2. Two possible configurations satisfying the nominal attitude requirements.

The first step taken is to express the components of the reference vectors, the sun and the ecliptic vector, in spacecraft coordinates. The sun, denoted (x_s, y_s, z_s) is obtained from Figure 1. We see that

$$y_s = -x_s \tan \theta_z \quad z_s = x_s \tan \theta_y \quad (1)$$

Knowing that x_s is a unit vector, we find

$$x_s^2 + y_s^2 + z_s^2 = 1 = x_s^2 (1 + \tan^2 \theta_y + \tan^2 \theta_z) \quad (2)$$

which gives

$$x_s = (1 + \tan^2 \theta_y + \tan^2 \theta_z)^{-1/2} \quad (3)$$

without ambiguity since the x-axis is sun pointing and therefore $x_s > 0$. The ecliptic vector is the intersection of the ecliptic plane and the spacecraft yz-plane and is easily located in spacecraft coordinates. From Figure 1,

$$\begin{aligned} x_e &= 0 \\ y_e &= \cos \theta_x \\ z_e &= -\sin \theta_x \end{aligned} \quad (4)$$

The z-component has a reversed sign since the roll angle is measured *from* the ecliptic vector by definition. (This angle is negative in Figure 1.) Another useful quantity is the angle between the sun and ecliptic vector

$$\cos \theta_{es} = x_s \cdot x_e \quad (5)$$

We next need to find the ECI coordinates of the two reference vectors. The sun position, denoted by (u_s, v_s, w_s) , can be found from any of the several solar ephemeris models. The right ascension and declination of the sun are given respectively by

$$\alpha_s = \tan^{-1} \frac{v_s}{u_s} \quad \delta_s = \sin^{-1} w_s \quad (6)$$

Now, since θ_{cs} is the same in both coordinate frames and since the declination of the ecliptic vector is zero by definition, we have

$$\begin{aligned} \cos \theta_{es} &= \cos \delta_s [\cos \alpha_s \cos \alpha_e + \sin \alpha_s \sin \alpha_e] \\ &= \cos \delta_s \cos(\alpha_s - \alpha_e) \end{aligned} \quad (7)$$

in which α_e is the right ascension of the ecliptic vector. Now, since $-\pi/2 < \delta_s < \pi/2$ and since for APEX, $\theta_{cs} \approx \pi/2$, we must admit to two solutions.

$$\alpha_e = \alpha_s \mp \cos^{-1}(\cos\theta_{es}/\cos\delta_s) \quad (8)$$

A look at Figure 2 shows that the subtractive case corresponds to configuration 1 and the additive case to configuration 2.

Now, the spacecraft frame basis vectors \mathbf{x}_s and \mathbf{x}_e are used to form an orthogonal set as follows

$$\begin{aligned} \mathbf{x}_1 &= \mathbf{x}_s \\ \mathbf{x}_2 &= \mathbf{x}_s \times \mathbf{x}_e / |\mathbf{x}_s \times \mathbf{x}_e| \\ \mathbf{x}_3 &= \mathbf{x}_1 \times \mathbf{x}_2 \end{aligned} \quad (9)$$

and the ECI vectors are used in the same way to form \mathbf{u}_1 , \mathbf{u}_2 and \mathbf{u}_3 . The two sets of vectors define a body matrix and a reference matrix

$$\mathbf{M}_B = [\mathbf{x}_1 : \mathbf{x}_2 : \mathbf{x}_3] \quad \mathbf{M}_R = [\mathbf{u}_1 : \mathbf{u}_2 : \mathbf{u}_3] \quad (10)$$

The attitude matrix $A_{s/c}$, consisting of the components of the spacecraft axes in ECI coordinates, will transform \mathbf{M}_R into \mathbf{M}_B

$$\mathbf{M}_B = A_{s/c} \mathbf{M}_R \quad (11)$$

and so the solution can be found.

$$A_{s/c} = [\mathbf{u}_{s/c} : \mathbf{v}_{s/c} : \mathbf{w}_{s/c}] = \mathbf{M}_B \mathbf{M}_R^T \quad (12)$$

This rather lengthy set of operations completely specifies the attitude of the spacecraft when given pitch, roll and yaw. We now turn to the opposite transformation.

2.2 CONVERSION FROM INERTIAL COORDINATES

Given $A_{s/c}$, the pointing directions of the three spacecraft axes in ECI coordinates, we can find the corresponding pitch, roll and yaw as follows. Using a model for the direction of the sun in ECI coordinates \mathbf{u}_s , we calculate the direction of the sun in the body frame.

$$\mathbf{x}_s = A_{s/c} \mathbf{u}_s \quad (13)$$

Then, quite clearly, from the definition

$$\theta_y = \tan^{-1} \frac{z_s}{x_s} \quad \theta_z = -\tan^{-1} \frac{y_s}{x_s} \quad (14)$$

Now, the reference ecliptic vector \mathbf{u}_e is perpendicular to the spacecraft x-axis $\mathbf{u}_{s/c}$ and in the ecliptic plane.

$$\mathbf{u}_e = (\mp \hat{k}) \times \mathbf{u}_{s/c} \quad (15)$$

where \hat{k} is the ECI unit vector and the ambiguity in sign again refers to configuration 1 (-) and configuration 2 (+). Then, since the rotation to be made is one around the spacecraft x-axis, to which both the spacecraft y-axis and \mathbf{u}_e are perpendicular, the angle can be calculated from the angular difference between the spacecraft y-axis $\mathbf{v}_{s/c}$ and the ecliptic vector \mathbf{u}_e

$$\theta_x = \cos^{-1}(\mathbf{v}_{s/c} \cdot \mathbf{u}_e) \quad (16)$$

The sign of θ_x again deserves attention. If we are in configuration 1 (configuration 2) and $y_{s/c}$ is above (below) the ecliptic plane, the sign is negative.

3.0 MODELING THE ATTITUDE

In order to provide a test data set for development of attitude solution algorithms, it is necessary to perform some sort of simulation of the environmental forces and control laws that will be used to maintain the attitude. This simulation should provide a test set that is qualitatively similar to the actual APEX attitude behavior. However, it is not the purpose of this work to assess the probable degree of attitude control. This is not even possible, since the control depends to a large extent on the control laws selected. Even at this point, these are subject to change. In fact, it may be even better if this simulation behaves more erratically than the actual satellite does, since this presents a greater challenge to the attitude determination algorithms. In this modeling, then, we will attempt to develop a self-consistent data set that *might* be typical of the APEX data, based on our present understanding of the control mechanisms.

3.1 EPHEMERIS MODELING

The first step toward modeling of the attitude and sensor data is the definition of an APEX orbit. The actual ephemeris, including satellite position and velocity, sun position and magnetic field in ECI coordinates, was generated from test element sets using the APEX Ephemeris Computation Program [McNeil, 1992]. The test elements, which are input to the Ephemeris Computation Program, were generated using the Artificial Satellite Analysis Program (ASAP) [Kwok, 1987]. Ephemeris files were generated for the first nine days of 1992 using a semi-major axis of 7572.75 km, an eccentricity of 0.1055, an inclination of 70°, argument of perigee and ascending node were set at 166° and 159.4° respectively. These nine days represent a good test of the system since they begin with no eclipses and end with roughly the longest eclipses that the satellite will experience. Eclipses that take place in these days occur slightly after apogee and are over before perigee is obtained. To make the test set more comprehensive, we

have added Case 10, which was generated by shifting the epoch of Case 1. During this day, eclipse takes place at perigee.

3.2 MODELING ENVIRONMENTAL TORQUES

The largest torque for the APEX satellite arises from atmospheric drag. In keeping with the simplicity of this simulation, we model the satellite as a cylinder of radius R and half-length L . Let \mathbf{v} be a unit vector in the spacecraft frame in the direction of the velocity and let the magnitude of the velocity be v_m . The cylinder has three surfaces. Assuming the center of gravity to be at the center of the cylinder, the pressure point for the side is

$$\mathbf{p}_s = (0 \quad R \cos \alpha_v \quad R \sin \alpha_v) \quad (17)$$

where $\alpha_v = \tan^{-1}(v_z/v_y)$. The force on this surface is

$$\mathbf{f}_s = -2 C_D \rho(h) v_m^2 L R \sqrt{1 - (\mathbf{v} \cdot \mathbf{n})^2} \mathbf{v} \quad (18)$$

where C_D is the drag coefficient and ρ is the atmospheric density at altitude h . The torque arising from this surface is

$$\boldsymbol{\tau}_s = -2 C_D \rho(h) v_m^2 L R^2 \sqrt{1 - v_x^2} (\sin \alpha_v v_x \hat{\mathbf{j}} - \cos \alpha_v v_x \hat{\mathbf{k}}) \quad (19)$$

For the top of the canister, whenever $v_x > 0$, the pressure point is

$$(L \quad 0 \quad 0) = \mathbf{p}_t \quad (20)$$

the force on this surface is

$$\mathbf{f}_t = -\frac{1}{2} C_D \rho(h) \pi R^2 v_m^2 (\mathbf{n} \cdot \mathbf{v}) \mathbf{v} \quad (21)$$

and the torque is given by

$$\boldsymbol{\tau}_t = \frac{1}{2} C_D \rho(h) \pi R^2 L v_m^2 v_x (v_z \hat{\mathbf{j}} - v_y \hat{\mathbf{k}}) \quad (22)$$

For the bottom of the canister, when $v_x < 0$, the sign of $\boldsymbol{\tau}_t$ is reversed.

We choose a density model with a simple exponential form

$$\rho(h) = \rho_0 e^{\frac{h_0 - h}{H}} \quad (23)$$

Choosing 200 km as the reference altitude, the 1976 US Standard Atmosphere gives $\rho_0 = 1.0(-10)$ kg/m³ and a scale height chosen to be $H = 54.3$ km extrapolates to a good representation of the mean neutral density for the APEX altitudes. This model gives a density of about 6(-12) kg/m³ at perigee.

Although the aerodynamic torque is strongest for APEX near perigee, the eccentricity of the orbit makes this torque insignificant over the greater part of the orbit when the atmospheric density drops by several orders of magnitude. The second strongest environmental torque, arising from the gravity gradient, is much more constant throughout the orbit and stronger than the aerodynamic torque most of the time. To an adequate approximation [Wertz, 1986], this torque is given by

$$\tau_G = \frac{3\mu}{R_s^3} \hat{r} \times (I \cdot \hat{r}) \quad (24)$$

where R_s is the satellite radius vector, \hat{r} is a unit vector along the radius vector in the spacecraft frame, I is the moment of inertia vector and the gravitational constant $\mu = 4(5)$ km³/s².

The magnitude of these torques are shown in Figure 3 for a series of typical APEX orbits. Since the environmental torques are quite small except near perigee, one might expect that the satellite would obtain near perfect sun-oriented attitude except perhaps during the perigee pass. We will see, however, that the nature of the control system leads to another situation where control becomes less than optimum.

3.3 MODELING CONTROL LAWS

Control laws are used to calculate commands to the torque rods and momentum wheel that drive the satellite toward the desired attitude. For APEX, these laws depend on the current values of pitch, roll and yaw and on the rates of change of these values. The control laws implemented in this work are taken from the 30 April 1992 version of Orbital Sciences' code for attitude determination and control. They are a coupled set of laws involving pitch, yaw and roll as well as momentum wheel speed. The desired torque rod commands are calculated from

$$\tau_x = -r_{11}\theta_x - r_{12}\frac{d\theta_x}{dt} - r_{13}\Delta s_w \quad (25)$$

Simulated APEX Environmental Torques

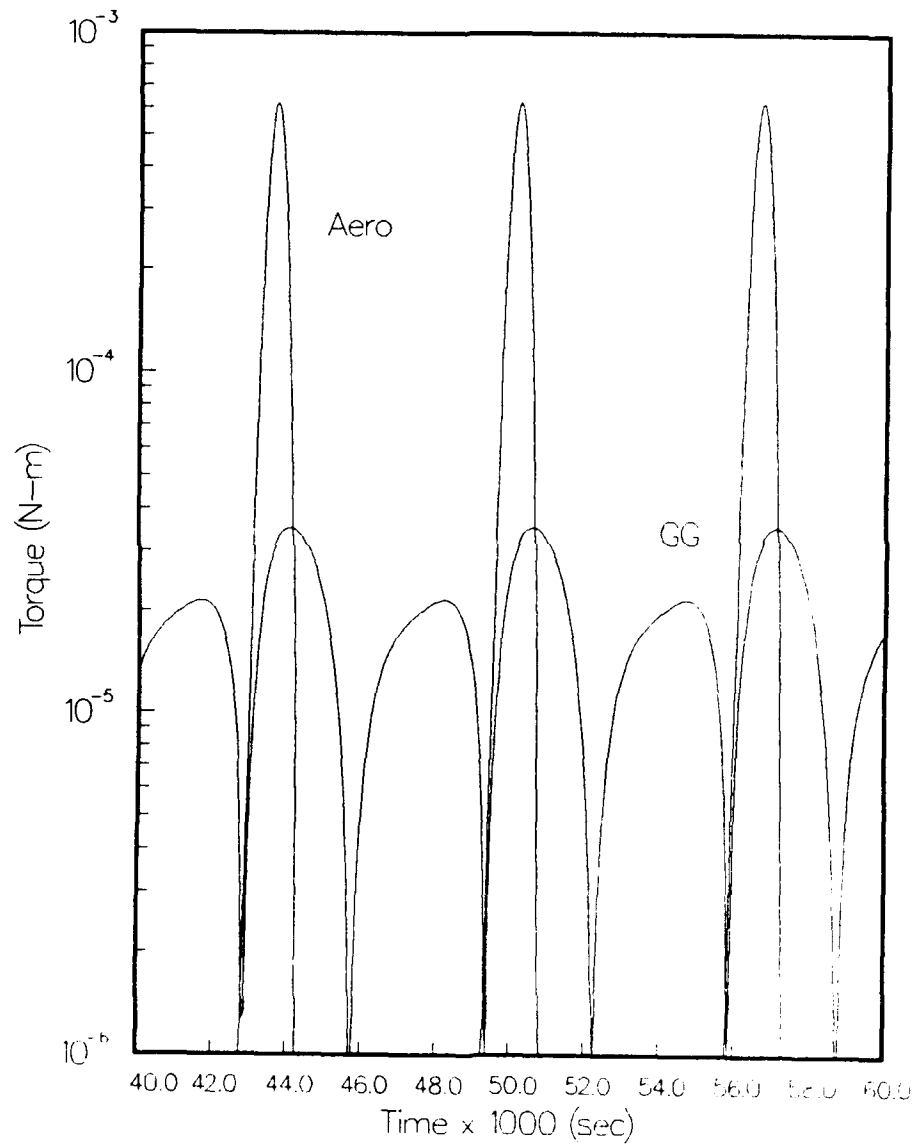


Figure 3. Simulated Aerodynamic (Aero) and Gravity Gradient (GG) Torques for the APEX Satellite.

where Δs_w is the deviation of the momentum speed from its desired speed. Commands to the y and z (pitch and yaw) torque rods are calculated from linear combinations of pitch and yaw rates as follows.

$$\begin{aligned}\tau_y &= -k_{11}\theta_y - k_{12}\frac{d\theta_y}{dt} - k_{13}\theta_z - k_{14}\frac{d\theta_z}{dt} \\ \tau_z &= -k_{21}\theta_y - k_{22}\frac{d\theta_y}{dt} - k_{23}\theta_z - k_{24}\frac{d\theta_z}{dt}\end{aligned}\quad (26)$$

It is not possible, however, to apply precisely these torques, since the actual torque will depend on the direction and magnitude of the external field. The moments to be applied to the torque rods are calculated from

$$\mathbf{M} = (|\mathbf{b}|^{-1})\hat{\mathbf{b}} \times \boldsymbol{\tau} \quad (27)$$

where $|\mathbf{b}|$ is the magnitude of the measured external field. If any of the components of \mathbf{M} exceed the maximum of 30 Amp-m², the torque is set to the maximum value for this axis. The torque rod torques arising from this moment are then

$$\boldsymbol{\tau}_c = \mathbf{M} \times \mathbf{b} \quad (28)$$

The command torque to the momentum wheel is calculated from the roll, the roll rate and the wheel speed as follows.

$$\tau_{mw} = -r_{21}\theta_x - r_{22}\frac{d\theta_x}{dt} - r_{23}\Delta s_w \quad (29)$$

The torque in the x-direction to the vehicle is the negative of this value. For the sake of simplicity, we will ignore changes in momentum wheel speed, taking Δs_w as zero throughout. The purpose of including the wheel speed in the control laws is to unload excess momentum. This is done quite slowly and, for practical purposes, only when the values of pitch, roll and yaw are small, during apogee passes when the aerodynamic torque is minimal. This process would probably not change the attitude appreciably. The coefficients used in the modeling are given in Table 1.

Table 1. Control Law Coefficients

k_{11}	0.0810	k_{12}	0.0725	k_{13}	2.9400	k_{14}	-0.0337
k_{21}	-0.0723	k_{22}	0.0808	k_{23}	0.0397	k_{24}	2.7030
r_{11}	2.19(-4)	r_{12}	7.19(-2)	r_{21}	-0.1870	r_{22}	-4.5600

3.4 INCLUDING MAGNETOMETER EFFECTS

In sunlight, the measured values of pitch and yaw and thus the attitude control of the sun angle is based on the sun sensor measurements alone. The roll angle, θ_x , is calculated by comparing magnetometer data to a model magnetic field. We wish to include the effects of errors in the calibration of that magnetometer in the simulation, at least in a simple way. Note that the roll angle reported by the satellite will *not* include errors in calibration. The reported roll reflects only the difference between where the spacecraft y-axis ought to be and where the spacecraft *thinks* the axis is. An error in calculation of the spacecraft magnetic field will displace both these angles by a factor that depends on the type of calibration error and on the orientation of the external magnetic field in the spacecraft frame.

We include a possible calibration error in the simulation by adding to the measured magnetic field a static internal field B_{ind} . It is quite difficult at this point to determine the precise nature or magnitude of B_{ind} in practice but, once chosen, the additional error in roll can be approximated as follows. Assuming that the pitch and yaw are accurately calculated from the sun sensor, the measured magnetic field will be

$$B_m = B_{ext} + B_{ind} \quad (30)$$

The induced field is made up of two components, a static part that represents a miscalibration of the instrument and which could be removed by on-orbit calibration methods, and a time varying part that arises from operational currents and which will probably not be compensable in the processing. The second of these is modeled by high frequency sine waves that simulate random noise. To mimic a random induced field, each axial component is determined from an amplitude and a period according to

$$B_{r,i} = B_r \sin(2\pi f_i T/P) \quad (31)$$

where f_i is taken to be 1.0, 1.1 and 1.2 for x, y and z respectively and where the period P is fixed during a simulation. According to the estimates of Orbital Science Corp. engineers [Barnison, 1992] the magnitude of this field is around 120 nT.

The static component warrants some extra attention and explanation. This represents a less than perfect knowledge of the 'average' offsets of the magnetometer both in the Attitude Determination and Control (ADC) system and in the Attitude and Magnetic Field Processing (AMP) system used to produce attitude and magnetic field data products. Errors in the offsets in the ADC will affect the attitude itself. We will investigate these errors in what follows, but generally we will assume that the magnitude of this miscalibration is on the order of the random component, perhaps 200 nT. We will not assume *a priori* knowledge of the offsets in the magnetic field calibration algorithms to be presented later. Thus so far as the AMP processing is concerned, the addition of a static offset does nothing more than change the values resulting from the calculation.

The effect of these induced fields on attitude control will probably be similar to the following. In the attitude determination and control code, the roll is calculated by projecting the measured and model magnetic fields into the spacecraft yz-plane and taking the angle between them. The induced field will thus lead to an angular error equal to

$$\epsilon_x = \pm \frac{B_{ym}B_{yext} + B_{zm}B_{zext}}{(B_{ym}^2 + B_{zm}^2)^{1/2} (B_{yext}^2 + B_{zext}^2)^{1/2}} \quad (32)$$

with the sign being determined by the cross product of the two. This error in the on-board attitude solution is simulated by modification of the value of θ_x in the control laws

$$\theta_x = \theta_x - \epsilon_x \quad (33)$$

3.5 ECLIPSE CONTROL LAWS

During eclipse, when data from the sun sensor is not available, the current attitude of all three axes is calculated from magnetometer data alone. The attitude control is no less efficient in eclipse than in sunlight, however, the error in attitude knowledge results in a pointing error depending on the accuracy of the magnetometer calibration and the specifics of the methods used to calculate attitude. We will ignore these specifics for simplicity's sake and model the effect by the subtraction of the values

$$\epsilon_y = \sin^{-1} \frac{B_{ind,y}}{B_{ext,yz}} \quad \epsilon_z = \sin^{-1} \frac{B_{ind,z}}{B_{ext,yz}} \quad (34)$$

from the values of θ_y and θ_z in the control laws during eclipse. b_{yz} is the projection of the magnetic field vector onto the spacecraft yz-plane. These are probably 'worst case' expressions for the angular error in that the error is taken to be the perpendicular component of the induced field and no filtering or complicated attitude calculation techniques are assumed.

3.6 EQUATIONS OF MOTION

The rotation rates about the three spacecraft axes, ω_i , vary in time according to

$$\frac{d}{dt} (I\omega) = \tau_{disturbance} + \tau_{control} - \omega \times I\omega - \omega \times h \quad (35)$$

where h is the angular momentum of the momentum wheel. Assuming that the moment of inertia tensor is diagonal, the tensor equations reduce to linear ones.

$$\begin{aligned}
I_x \frac{d\omega_x}{dt} &= \tau_x - (I_z - I_y)\omega_y\omega_z \\
I_y \frac{d\omega_y}{dt} &= \tau_y + (I_z - I_x)\omega_x\omega_z + h\omega_z \\
I_z \frac{d\omega_z}{dt} &= \tau_z - (I_y - I_x)\omega_y\omega_x - h\omega_y
\end{aligned} \tag{36}$$

The moments of inertia used are as follows.

$$I_x = 49 \text{ km-m}^2 \quad I_y = 72 \text{ km-m}^2 \quad I_z = 61 \text{ kg-m}^2$$

The momentum wheel angular momentum, entirely in the spacecraft x-direction, is taken at 4 Nms. Beginning with $\omega=0$ we can follow the evolution of θ through

$$\frac{d\theta_x}{dt} = \omega_x \quad \frac{d\theta_y}{dt} = \omega_y \quad \frac{d\theta_z}{dt} = \omega_z \tag{37}$$

These relations are not quite correct since θ_x , θ_y , and θ_z are measured in a system that is not quite inertial. However, since the motion of the sun in the inertial system is quite small on time scales of the attitude changes, this formulation should suffice. These equations are coupled since the torques depend upon the θ angles. They can be solved by any standard technique for differential equations. We choose a fourth-order Runge-Kutta for this work. Following the intended scheme in the actual spacecraft, the attitude is sampled for one-fifth second then driven with the torque rods and momentum wheel for the remainder of the second.

3.7 SIMULATION RESULTS

In this section, we discuss some of the important features that derive from the model discussed above. First, in Figure 4, we show pitch and yaw for a series of about three orbits which are entirely sunlit. The attitude angles exhibit their greatest deviation at perigee, and the degree of this deviation is to some extent dependent on the direction of the external magnetic field. This arises because correction of pitch and yaw errors becomes increasingly more difficult when the magnetic field lies near the spacecraft yz-plane. One sees some substantial deviations even near apogee when this is the case. The bottom panel gives the ratio of x-axis field to total field. The legend in that and the following figures should be interpreted as follows: T_c is the control period in seconds, T_s is the sampling period in seconds, B_i is the static induced magnetic field, B_r is the "random" induced magnetic field and P is the period of the random field in seconds.

In Figure 5, we show the roll axis angle for the same time period with various magnitudes and frequencies of the time varying induced fields. The bottom panel shows the case with no

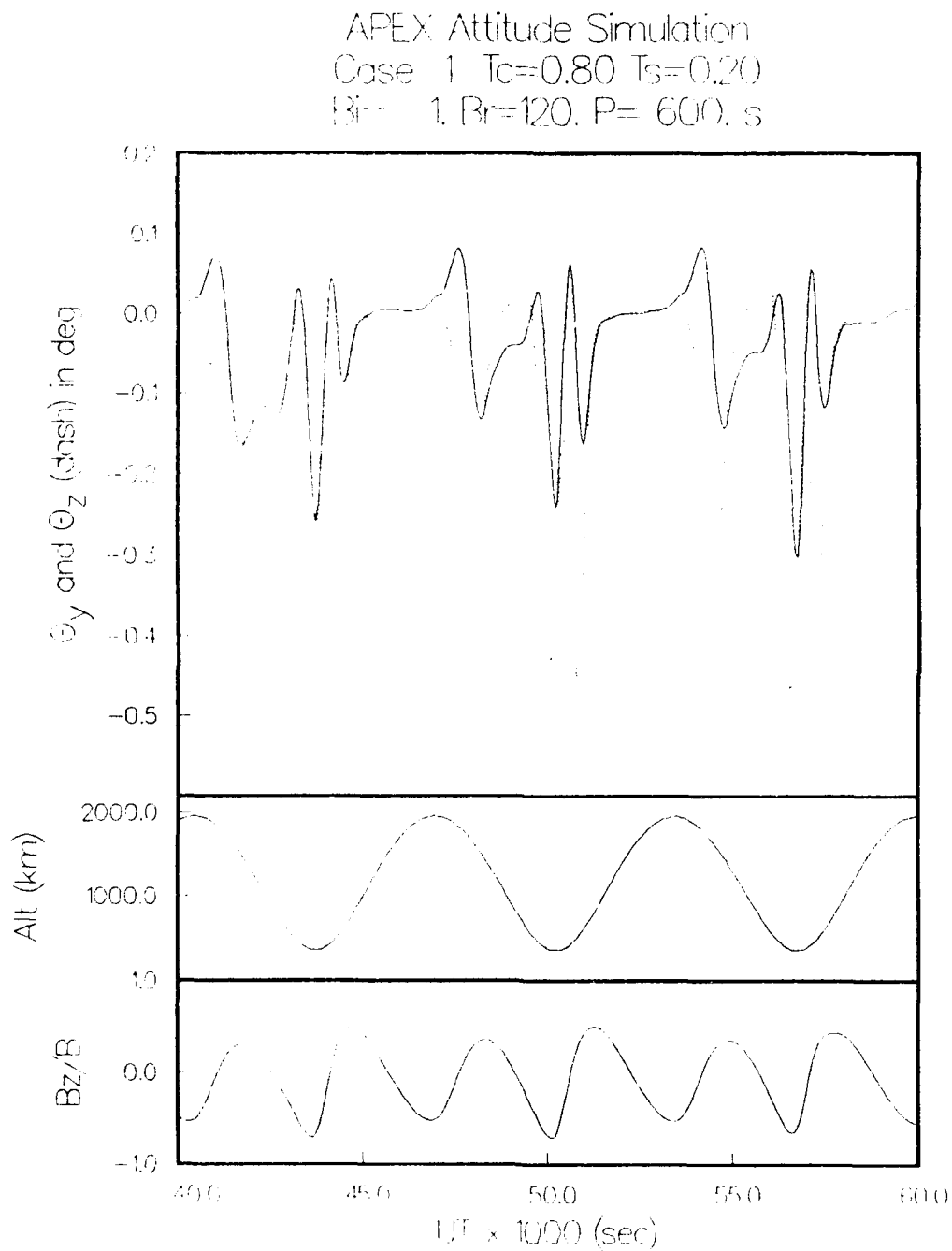


Figure 4. Typical pitch and yaw (sun directed) angles during sunlit operation.

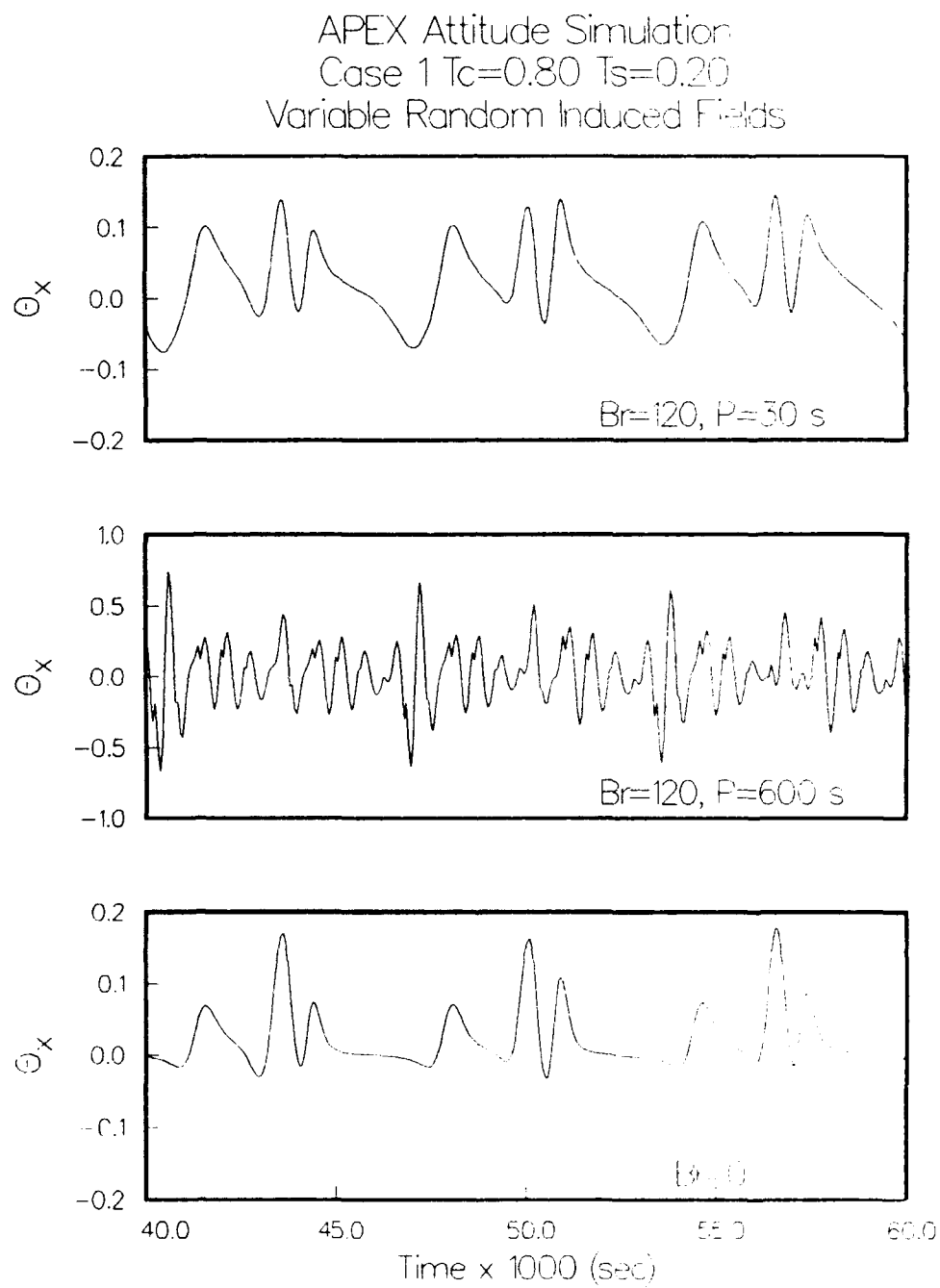


Figure 5. Values of roll axis attitude with low and high frequency induced fields.

induced field. Here, the roll follows a pattern much the same as pitch and yaw with the exception that the deviations from nominal operation (roll equals zero) are less severe. This is because roll control is based mainly on momentum wheel speed changes and is thus more easily controlled. The second panel, with time varying induced fields of 120 nT with period of 10 minutes, shows deviations from zero that can be thought of as arising mostly from errors in the calculated attitude (roll) due to the induced field. It is important to keep in mind that the magnitude of the control error is dependent entirely on the magnitude of the induced field and, should induced fields turn out to be larger than expected, errors in control and in calculation of the attitude would be larger as well. Another interesting result is seen in the top panel of Figure 5, where we have chosen a frequency less than the response time of the attitude control system. In this case, the roll remains nearer the desired value since the induced field has fluctuated in the other direction before the satellite has had time to respond to the erroneous measured field.

Figure 6 shows the roll attitude for induced fields (calibration errors) of 100, 200 and 500 nT. The magnitude of the error of any particular point is a function of the direction of the external field and its magnitude. As a rule of thumb, however, errors can reach $\sin^{-1}(b_i/b_{yz})$ where b_i is the induced field and b_{yz} the magnitude of the external field in the yz plane of the spacecraft. This relation applies equally well to the time varying fields. The essential difference between time varying and static fields is, again, that there is some hope of removing static fields through calibration. Time varying fields, on the other hand, will be more or less invisible to the attitude user since it will be impossible to distinguish between actual roll errors and errors introduced by dynamic fields. We note that the filtering and weighting techniques employed in the on-board solution will almost certainly reduce these errors in practice.

For completeness, we show in Figure 7 the calculated torque rod commands that give rise to the attitude control shown in the previous figures. The torque rods are maximum near apogee and at times when the magnetic field is nearly perpendicular to the spacecraft x-axis, as discussed previously. The maximum torques do not exceed the 30 A-m² limit imposed by their design.

Finally, in Figure 8 we show the pitch and yaw angles during a series of orbits in which there is an eclipse. The eclipse period is shown by negative values of the solar depression angle in the bottom panel. The roll angle in this case is not substantially different from those shown previously. This is merely one example of what the attitude behavior might be during eclipse, and substantial variations may be expected due to position of the eclipse within the orbit and the magnitude and time dependence of the induced fields. First, there is a sharp transition from high precision sunlit attitude control to eclipse attitude control. This is reasonable since the attitude is controlled with relatively high precision by the attitude values calculated on-board. These change discontinuously as eclipse is entered due to the errors introduced by induced fields. More importantly perhaps is the realization that the excursions of the attitude from nominal values during eclipse is dependent mainly on the induced fields. Since these cannot be well predicted at this point, and since attitude determination during eclipse must necessarily involve the parameterization of the attitude behavior over time, it would seem best to limit *a priori* assumptions about the attitude behavior as much as possible. We return to this point when we discuss the attitude solution in eclipse.

APEX Attitude Simulation
Case 1 $T_c=0.80$ $T_s=0.20$
Variable Static Induced Fields

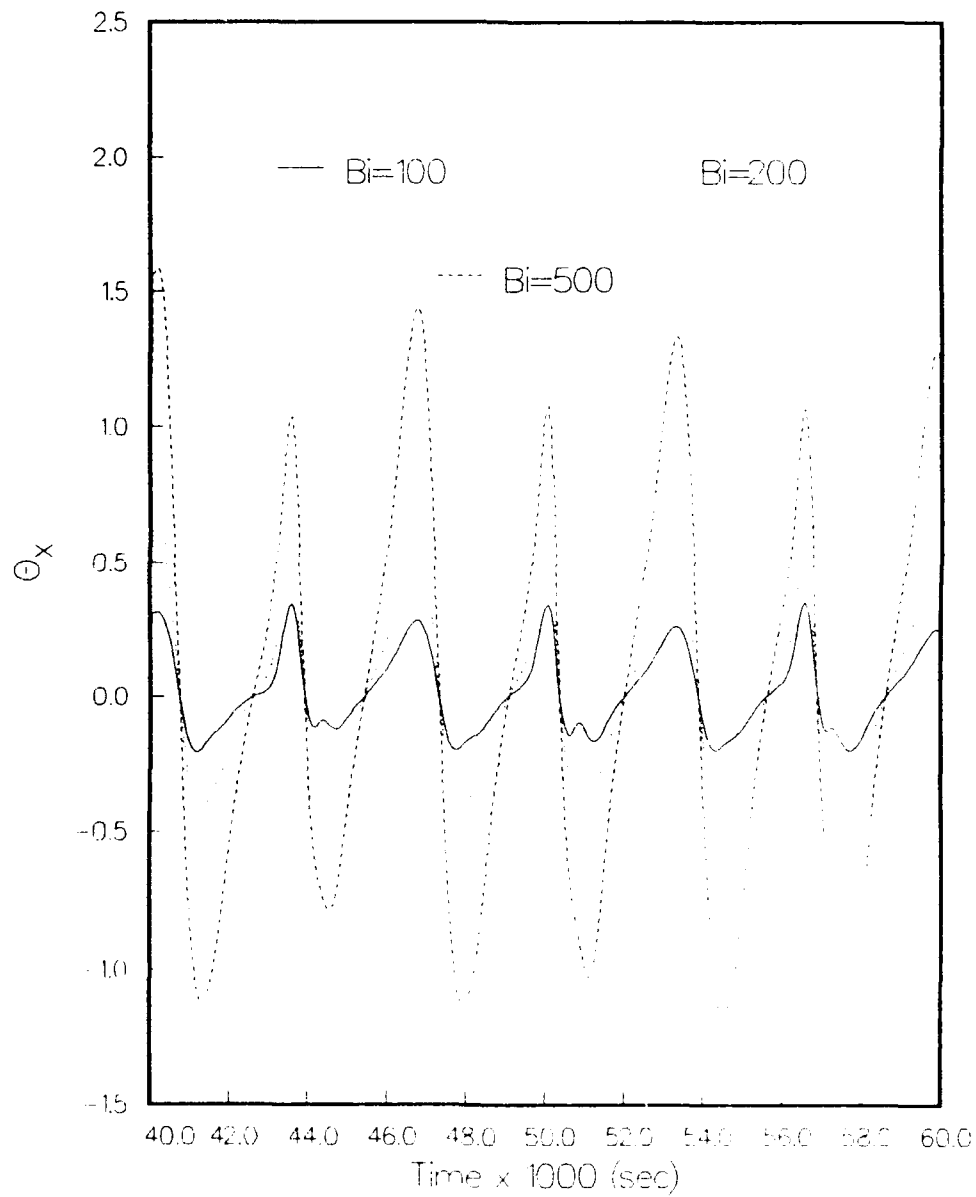


Figure 6. Roll axis attitude with various static induced fields.

APEDX Attitude Simulation
 Case 1: $I_x=0.80$, $I_y=0.24$
 $E^2=500$, $B=120$, $P=150$ s

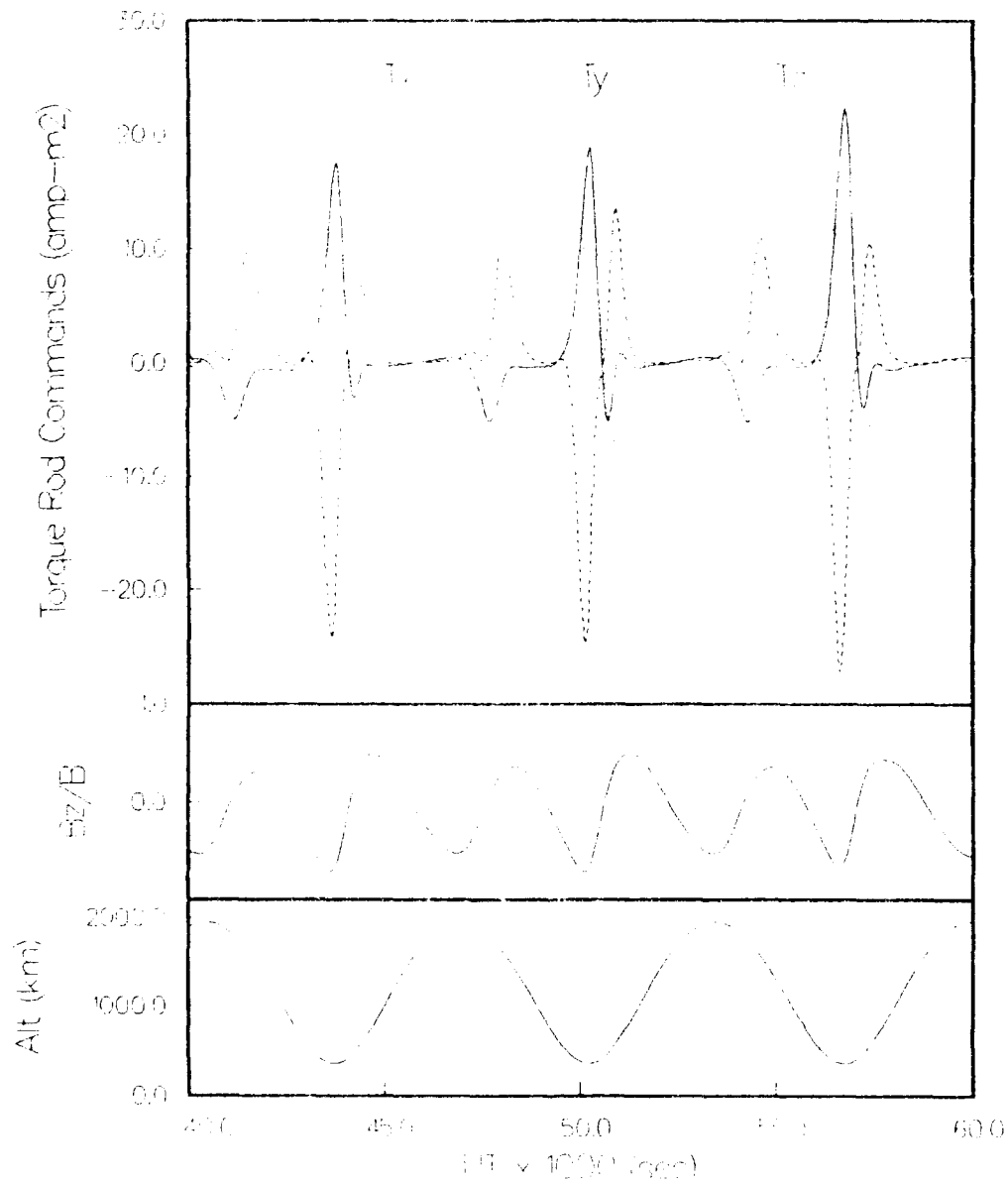


Figure 7. Torque Rod Commands.

APEX Attitude Simulation
Case 9 $T_c=0.80$ $T_s=0.20$
 $Bi=200$, $Br=120$, $P=30$ s

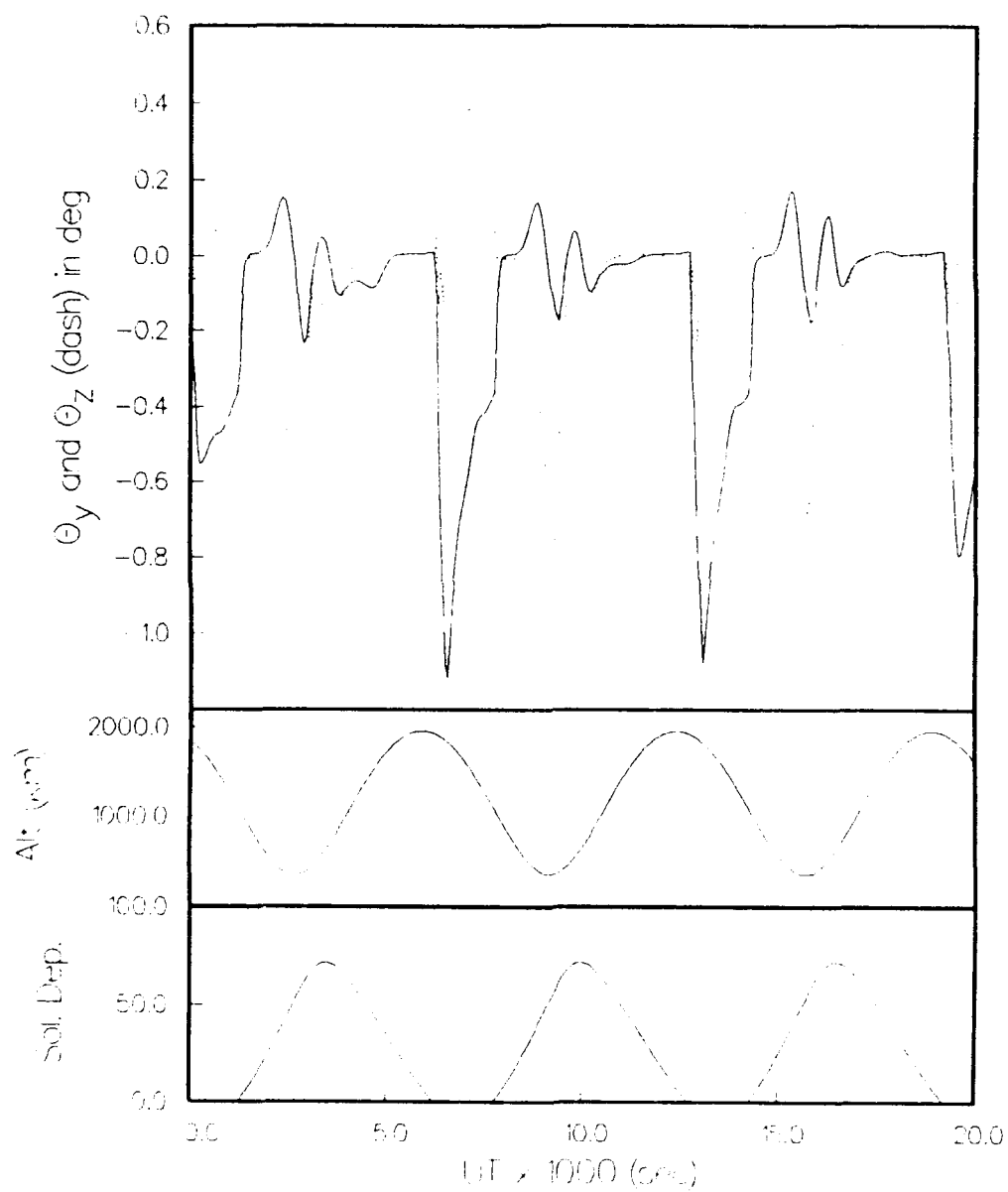


Figure 8. Pitch and yaw angles for an orbit with eclipses.

3.8 SIMULATION OF INSTRUMENTS

The simulation of the data stream from the satellite is quite straightforward, given the assumptions of this model. The times chosen are 60 seconds apart at some arbitrary whole second. All measurements are assumed to be coincident in time. The magnetometer values are derived from

$$M_i = TRUNC([b_{m,i} + b_{ind,i} + 60000.0] / g_i + 0.5) \quad (38)$$

where TRUNC reduces the number to the nearest integer of lesser value. g_i is the gain factor for the magnetometer axis in nT/count. In this work, we will make the assumption that all gain factors are equal, but that the gain factor is unknown. As some justification, we cite the magnetometer aboard CRRES. There, gains were matched to approximately .08 nT/count with gains at approximately 22 nT/count. In a field of 30,000 nT, this amounts to approximately one hundred nT maximum, which is near the expected noise level of the system. Should it appear from ground test data, however, that the gains of the instrument are substantially mismatched, the calibration algorithms could easily be modified by multiplication of two of the sensors by the ground measured ratios. The nominal gain of the instrument is 1.831 nT/count.

The sun sensor values are taken directly from the values of pitch and yaw, since these are direct measurements for APEX. The natural measurements of the sun sensors are [Space Sciences, 1991] the tangents of the angles

$$r_y = -\tan\theta_z \quad r_z = \tan\theta_y \quad (39)$$

The full scale value of the sun sensor N is 20479 and the digital signal produced is

$$n = TRUNC(r / \delta + 10240 + 0.5) \quad (40)$$

where

$$\delta = \frac{2 \tan\theta_{\max}}{N+1} = 2.002450(-4) \quad (41)$$

when θ_{\max} is 64° . The sun sensor values are inserted in the simulated telemetry whenever the solar depression angle is greater than zero. Also produced is a flag which indicates whether the sun sensor can see the sun.

4.0 ATTITUDE SOLUTION ALGORITHMS

Having simulated the satellite orbit, attitude and instrument readings, we now turn to algorithms for processing these signals. Attitude solutions for APEX come entirely from combinations of sun sensor and magnetometer readings. In sunlight, the pitch and yaw angles are measured directly from the sun sensor data, with roll being calculated from these angles and the magnetic field measurements. In eclipse, all three axes are calculated from magnetometer data alone. Hence, it should be apparent that the calibration of the magnetometer is of critical importance in the enhancement of the accuracy of the attitude calculations. We deal with this issue first.

4.1 MAGNETOMETER CALIBRATION

In our simulation, the magnetometer is assumed to be aligned perfectly with the spacecraft axes, but to have unknown offsets, different for all three axes, and an unknown gain factor, which is equal for all three axes. The measured counts in each axis will be converted to the field in nT along the axis through the expression

$$b_i = M_i * g - d_i \quad (42)$$

We are somewhat limited in the use of on-orbit calibration methods by the fact that the satellite does not spin and remains more or less fixed inertially in all three axes. Calibrations can be carried out by comparison of the magnitude of the measured field with a model field. This method involves minimization of the function

$$F(g, d_x, d_y, d_z) = \sum [b_m^2 - (gM_x - d_x)^2 - (gM_y - d_y)^2 - (gM_z - d_z)^2]^2 \quad (43)$$

with respect g and the d_i 's, where b_m is the magnitude of a model for the field at the satellite position. In principle, a single minimization could be carried out on all four variables, however, the problem is better conditioned if we alternate between minimization of the gain g and the offsets d_i . Minimization is carried out by finding the zero of

$$-\frac{1}{4} \frac{dF}{dg} = f_g = \sum [b_m^2 - (gM_x - d_x)^2 - (gM_y - d_y)^2 - (gM_z - d_z)^2] \times [(gM_x - d_x)M_x + (gM_y - d_y)M_y + (gM_z - d_z)M_z] \quad (44)$$

for the gain and

$$-\frac{1}{4} \frac{dF}{dd_x} = f_x = \sum b_m^2 (gM_x - d_x) - \sum (gM_x - d_x)^3 - \sum (gM_x - d_x)(gM_y - d_y)^2 - \sum (gM_x - d_x)(gM_z - d_z)^2 \quad (45)$$

for the offsets. These are quite easily carried out by a Newton-Raphson search technique.

In order to test this algorithm, we selected a relatively short portion of data comprising about three orbits. Static induced fields were set at about 200 nT and random high frequency fields at 120 nT along each axis. The procedure would most likely be carried out infrequently over small portions of a day's data, as was done here. The calculation took initial guesses of $g = 1.8$ nT/count and $d_i = 60,000$ nT. Figure 9 shows the difference in measured and model field with calibrated and uncalibrated results. The header shows that the gain is calculated to better than 1 part in 2000. The values of d_i in the header represent 60,000 *plus* the static induced field (or calibration error). The twice-per-orbit oscillation in the lower uncalibrated panel is the effect on which the calibration algorithm relies. It is the result of variation in the direction of the background field with respect to the induced field, which stays relatively constant in inertial space.

It is perhaps not too impressive at first glance that calibration has reduced the error from a maximum of 300 nT to 150 nT or so, however, the 150 nT error in the top panel is almost entirely the result of the time varying induced fields, which we were never expecting to remove. Also, it is satisfying to note that the method works when static fields (calibration errors) are not significantly larger than the random components. A second example is shown in Figure 10. Here, we have assumed a static component of 500 nT in magnitude. For reference, static induced fields on the CRRES satellite were measured at around 200 nT in magnitude. CRRES was, however, a particularly clean satellite. On the other hand, the magnetometer on APEX is situated 24'' from the payload shelf, which reduces magnetic contamination. In practice, the differentiation between static and variable fields may not be straightforward. It may well turn out that certain long period events, such as ground transmission, cause large static fields during the duration. It is possible that these events could be identified in telemetry, and calibration could be carried both with and without, giving an extra set of offsets that could be used during the interval to improve the resulting magnetic field and attitude.

We should take note of a couple more things in relation to magnetometer calibration. First, plots like Figure 9 can be very useful in assessing the magnitude and frequency of induced fields, which we have seen can effect attitude control and which will turn out to be important in the assessment of the accuracy of the attitude determination. A final point pertains to alignment errors in the instrument. The procedure above does not rely on the alignment of the instrument with any particular spacecraft axis, but the resulting attitude and measured magnetic field when used to calculate pitch angle certainly do. We do not propose on-orbit calibrations for alignments. However, alignment test results should be available with which one can put upper bounds on the errors. Presumably, these will be insignificant. For reference, the engineering magnetometer aboard CRRES was aligned to about one-quarter degree.

4.2 ATTITUDE SOLUTIONS IN SUN LIGHT

When the satellite is in full sun, we have at our disposal two measured vectors in the spacecraft frame, the sun and the magnetic field. A straightforward and standard technique [Wertz, 1978] that can be used for three-axis attitude in this case is as follows:

APEX Magnetic Field Calibration
 $G=.830865$ $Dx=60098$ $Dy=60038$ $Dz=59835$

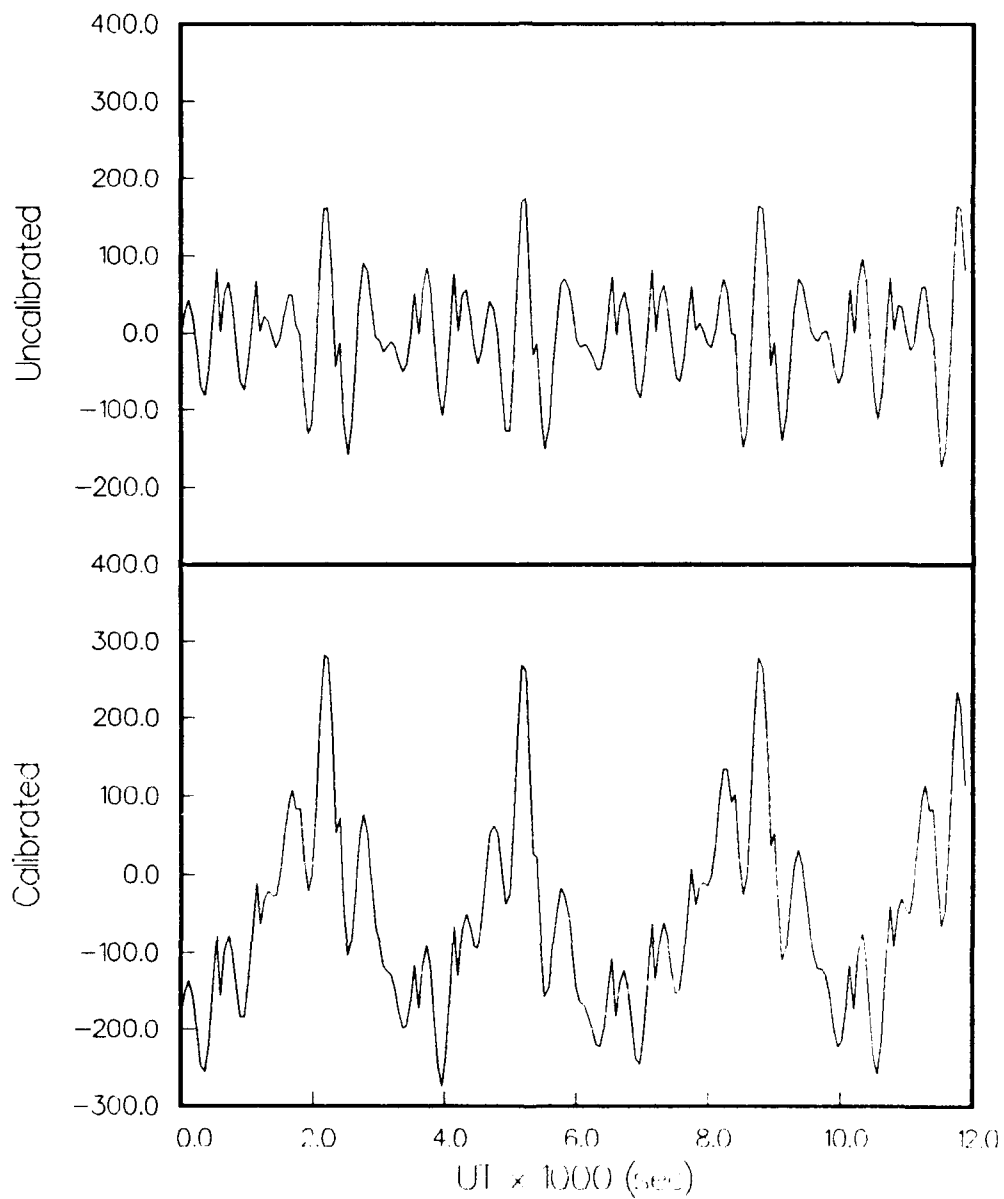


Figure 9. Difference between measured and model field with a 200 nT induced field.

APEX Magnetic Field Calibration
G=1.810858 Dx=60254 Dy=-60111 Dz=59588

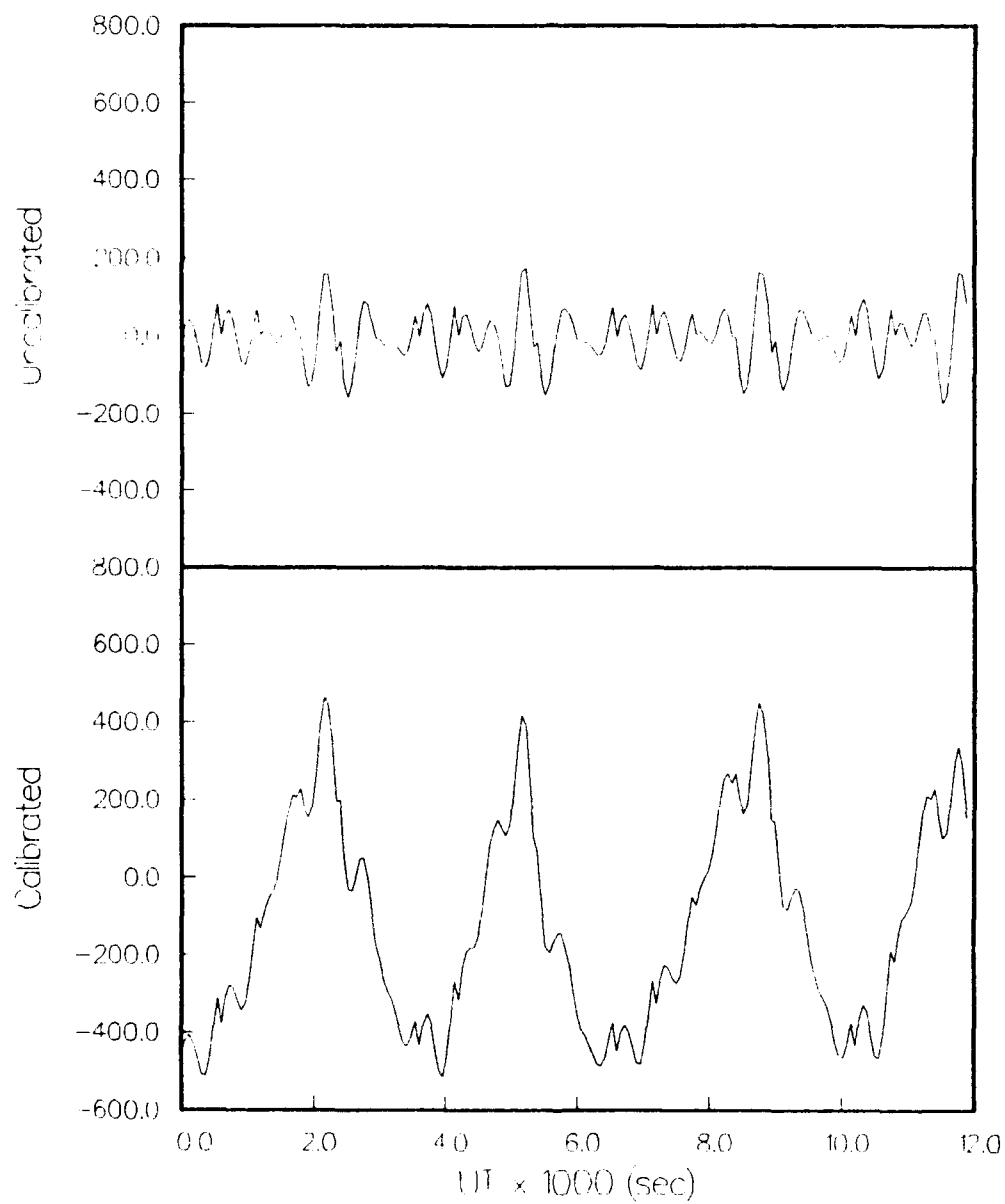


Figure 10. Same as Figure 9 but with a 500 nT induced field.

A triad of vectors is formed from the sun vector \hat{s} and the magnetic field vector \hat{b}

$$\begin{aligned}\hat{u} &= \hat{s} \\ \hat{v} &= \hat{s} \times \hat{b} / |\hat{s} \times \hat{b}| \\ \hat{w} &= \hat{u} \times \hat{v}\end{aligned}\tag{46}$$

in both the body frame (B) and, using models for sun and magnetic field vectors, in the inertial frame (I). Forming the matrices

$$M_B = [u_B : v_B : w_B] \quad M_I = [u_I : v_I : w_I]\tag{47}$$

we can specify the attitude matrix completely by

$$A M_I = M_B\tag{48}$$

and because of orthogonality

$$A = M_B M_I^T\tag{49}$$

giving a simple and unique solution for the attitude. From there, the results of §2.2 can be used to obtain pitch, yaw and roll. Since we use the sun vector as a basis vector, the resulting pitch and yaw are identical to the measurements of the sun sensor and the inherent high accuracy of these measurements has been preserved by the algorithm.

We should note that the OSC algorithm for calculation of roll angle in sunlight differs slightly from the one presented above [Orbital Sciences, 1992]. Their method involves calculating the angle between the magnetic field measured in the yz-plane and the field in a sun and ecliptic coordinate system. The two methods become identical when the satellite x-axis points directly at the sun and the difference in roll is negligible whenever the values of pitch and yaw are less than a few degrees.

To explore the results of this algorithm on the simulated data, we chose a relatively strong static induced field of 500 nT and a 120 nT time varying field with frequency high enough so that the field appears as noise in the magnetometer data. Figure 11 shows the pitch and yaw angles that result from the above scheme and the deviations of these results from the actual pitch and yaw. The errors are near the noise level of the sun sensor, since these are direct measurements. The uncertainty in the values of pitch and yaw during sunlit operation, then, will be limited by the resolution of the sun sensor. In practice, this limitation would also include mounting errors. Judging from measurements of the alignments for the CRRES satellite [Ball Aerospace, 1990] it would appear that typical values for this error are somewhat less than 0.2°. Since this is much greater than the resolution of the instrument, we will assign a probable uncertainty of pitch and yaw in sunlight to around 0.2°.

APEX Attitude — Case 2
Bi= 500. Br=120. P=3.5

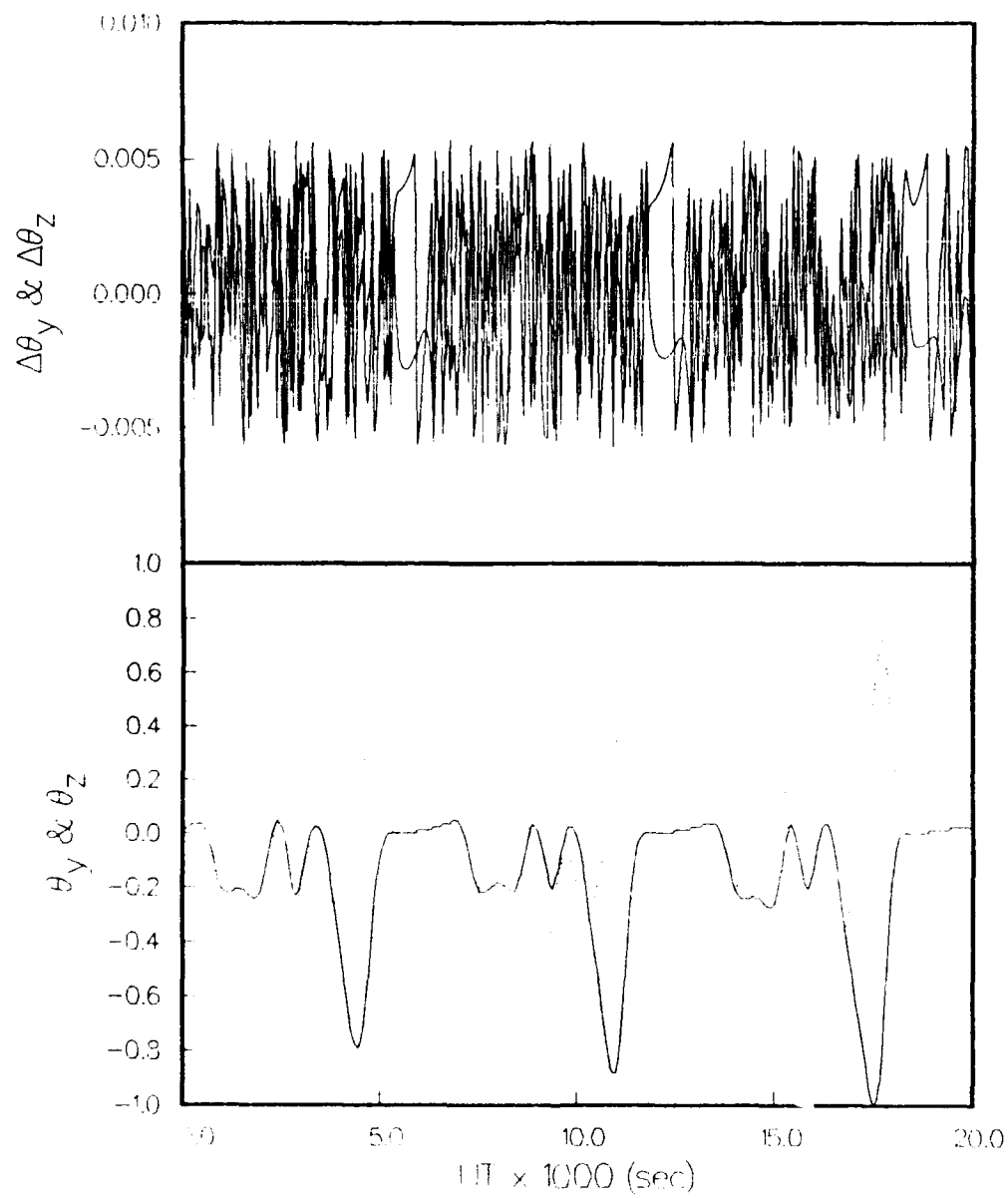


Figure 11. Pitch and yaw angles and errors, computed in sunlit operation.

Moving on to the roll axis, we show in Figure 12 the roll angle during the same period. Concentrating first on the actual roll, we see that the static field of 500 nT has introduced a control error of up to four degrees in roll. A notable aspect, though, is that when roll is calculated *without* correction for this static field, the value of roll appears to be *substantially better than it actually is*. This is because the same erroneous offsets were used in the control and in the calculation. This result emphasizes the importance of adequate magnetometer calibration for attitude knowledge, and points out the danger inherent in the use of on-board solutions without verification. Moving on to the calibrated solution, we see another interesting result. Although the solution is in agreement with the actual roll *on average*, it exhibits the same sort of random jumps as does the uncalibrated solution. This is due to the time varying induced field component, which is not removed by calibration. It is interesting that the actual roll does not undergo these oscillations. As discussed before, the control mechanism acts as a filter for high frequency modulations whenever the period is shorter than the time it takes the system to correct for an attitude error. Finally in Figure 13 we show the error in the roll calculation for this case, using the calibrated magnetic field data. The degree or so error is typical of the maximum effect of a 120 nT field.

It appears, then, that we are able to calculate the roll axis in sunlight to an accuracy limited by the "unremovable" spacecraft induced fields. It should be kept in mind, though, that the magnitude of these fields are at present unknown. The case presented above is unique to an induced field of around 100 nT. Repeating the above case with values of B_r set at 200 and 500 nT leads to maximum errors of 2.5° and 5.0° respectively. The nature of the "unremovable" induced field can be inferred to some degree from compatibility tests as well as on-orbit evaluations by observation of the variation of the measured magnetic field values.

Another issue of importance so far as error analysis is concerned arises from errors in the ephemeris and/or timing of the measurements. Whenever a relatively rapidly changing vector, such as the magnetic field, is used for reference, there is an error relating to the difference in calculated position and time and actual position and time. This is quite easy to investigate in the simulation by substituting the magnetic field calculated for a later time in the attitude determination. Figure 14 shows the results of this investigation. Figure 14 was generated with no induced fields at all, so we would expect all the error to be due to timing. This figure also serves to demonstrate the integrity of the simulation and calculation, since it shows an extremely small deviation due to the 1.8 nT resolution of the magnetometer in the simulation. For 1 and 2 second errors in timing, we see maximum errors of around 0.2 and 0.5 degrees respectively. For reference, the accuracy of the ephemeris will probably exceed 5 km in-track error [McNeil, 1992]. This puts the probable error from this source at around 0.1 degree maximum, since it amounts to about one-half second timing error.

Finally, the issue of the accuracy of the model field is always of importance when dealing with attitude derived from magnetometer measurements. It is our belief that a full IGRF model field extrapolated to date yields a field vector that is accurate to about 0.1° below, say, 4000 km or so. However, there are others who would set this error as high as 1.0° . Attempting to combine these error sources yields but one unknown, the "unremovable" induced fields. Using CRRES

APEX Attitude -- Case 2
Bi= 500. Br=120. P= 3. s

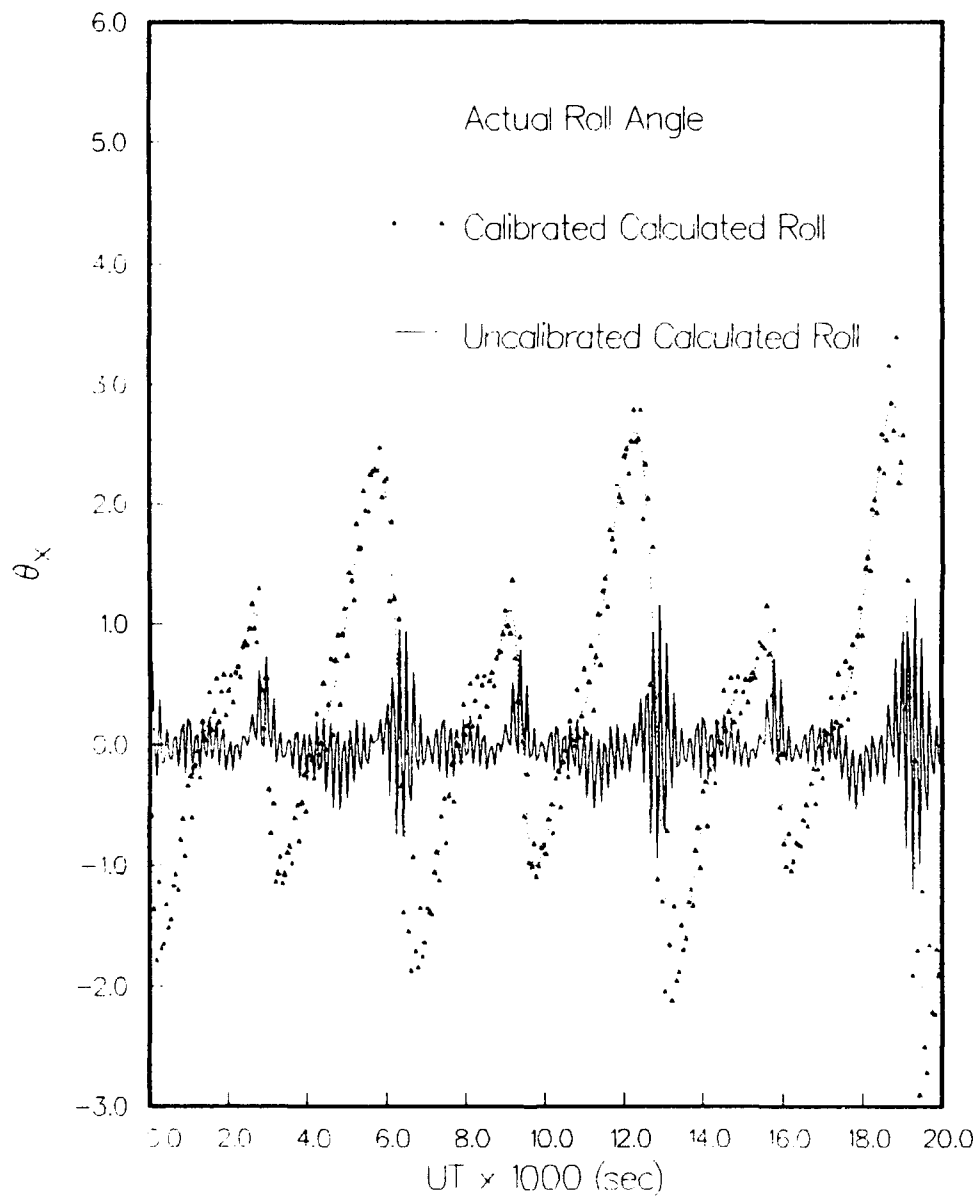


Figure 12. Roll axis angle, actual and calculated with and without calibration.

APEX Attitude - Case 2
Bi= 500. Br=120. P=3. s

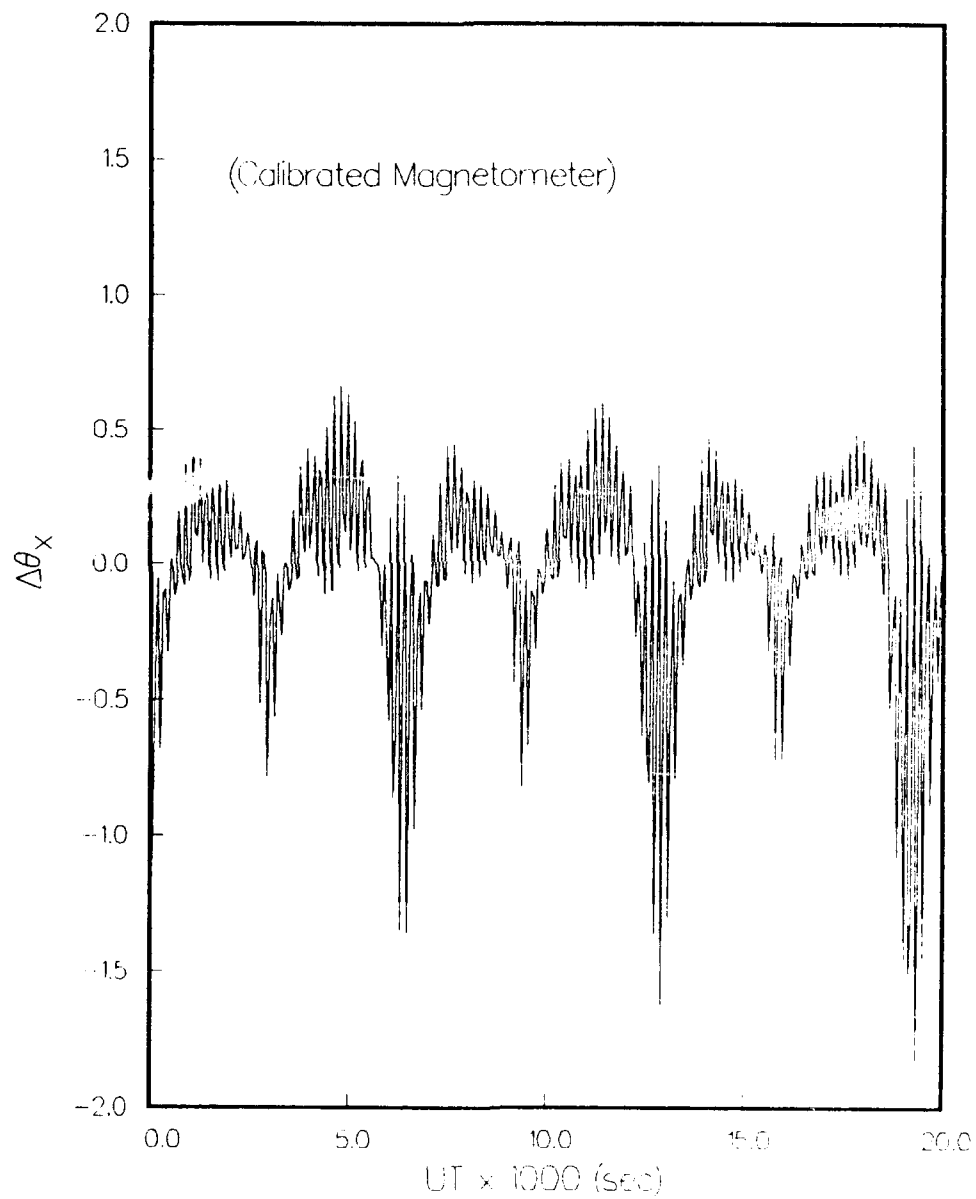


Figure 13. Roll axis error in sunlight with calibrated magnetometer.

APEX Attitude - Case 3
 $B_1 = 0$, $B_2 = 0$, $P = 3$ s

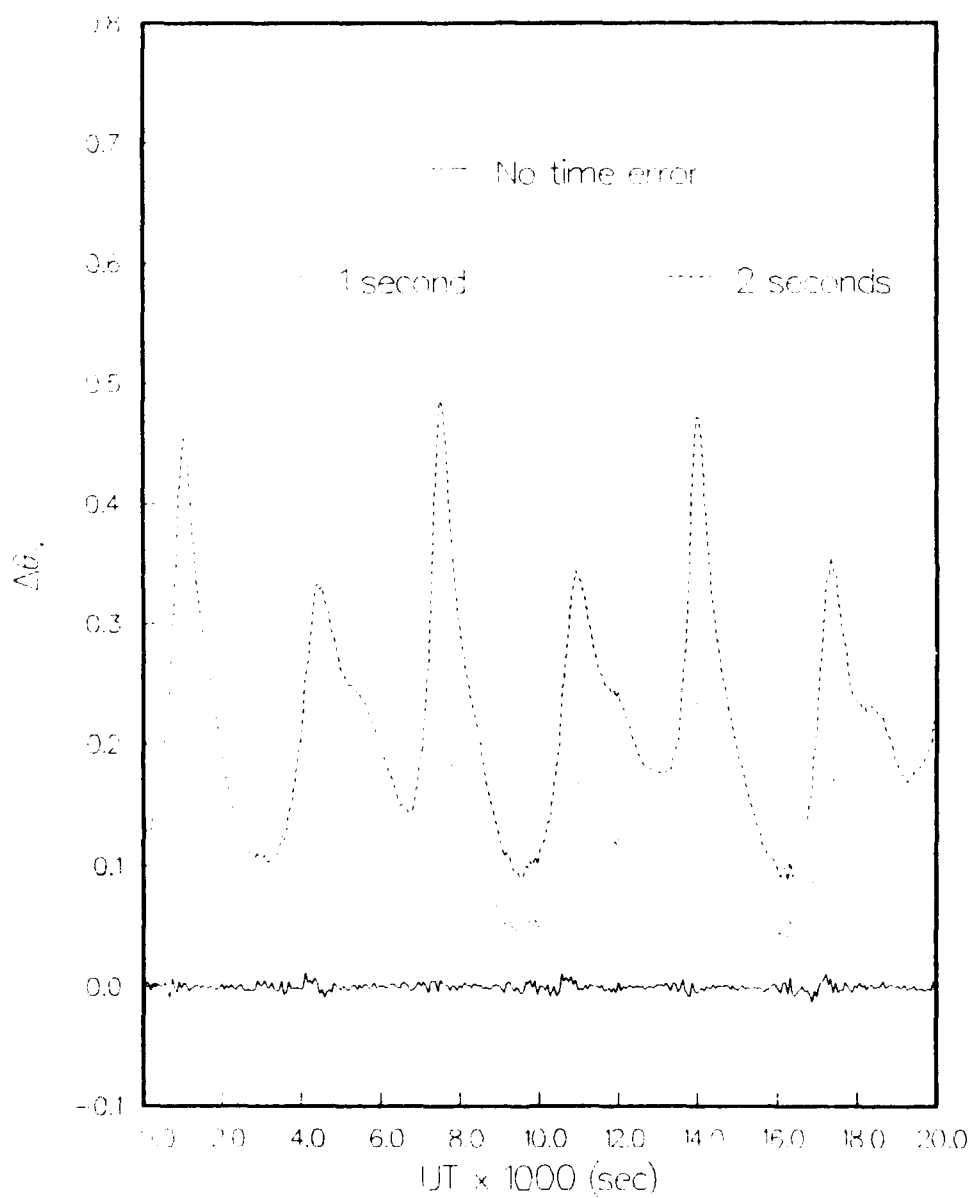


Figure 14. Roll axis error arising from errors in timing or ephemeris

again as a reference, the fields will be something around 100 nT at the magnetometer. Adding the ever present mounting error of 0.2° and taking the higher of the estimates for model field error, we find that the error in the calculated roll in sunlight may reach as high as 3° .

4.3 ATTITUDE SOLUTIONS IN ECLIPSE

Before describing a solution method for the attitude during eclipse, let us take a closer look at the attitude behavior. Figure 15 shows pitch, yaw and roll during one typical eclipse and slightly before and after. The eclipse actually begins at around 6200 seconds and ends at about 7600 seconds. A rather large static induced field of 500 nT was chosen for this run in order to accentuate the deviations from nominal operation. As the satellite enters eclipse, we see the effects of induced field in larger deviations in the pitch and yaw. Of note, however, is the fact that these deviations are relatively smoothly varying in time, depending for the most part on the direction of the magnetic field relative to the spacecraft. After entering sunlight again, we see that the control mechanisms require about four minutes to return pitch and yaw to near zero.

One of the most important aspects of the attitude solution during eclipse is that the only reference vector available is the measured magnetic field. One reference vector is not enough to uniquely specify the attitude at any moment. Therefore, a series of measurements must be combined to yield an attitude estimate. There are two popular methods of doing this [Wertz, 1986]. These are batch estimators and Kalman filters. In a batch estimator, a model of the observations, in this case the magnetometer readings taken during a certain period of time, is created from a parameterized state vector $x(t)$. These model measurements $g_i(x(t_i))$, are then compared to the actual measurements y_i . The loss function

$$J = \sum_i [y_i - g_i(x(t_i))]^2 \quad (50)$$

is minimized with respect to the state vector x in its particular parameterization. The model may vary in complexity from a constant attitude to one which includes derivatives of the state vector based on modeled environmental and control torques. The Kalman filter estimates the state vector $x(t_k)$ based upon the measurements y_i up to and including y_k , and on changes modeled and/or measured in the state vector between measurements.

We have opted for the batch least-squares approach for several reasons, although a Kalman filter will be used for on-board attitude calculation. First, we have seen that an induced field can lead to a relatively rapid change in attitude at the beginning of eclipses. Since the Kalman filter would require pre-eclipse data while the least-squares would not, using the later relieves us from any problems arising from a sudden attitude change. Also, in processing data by APEX periods, which may well begin or end in eclipse, a Kalman filter would require us to save data from other periods and to process sequentially while a least squares type would not. Finally, since post-flight attitude computation is intended mainly for verification of the on-board attitude, it makes some sense to employ an entirely different method because, as we have seen, attitude calculation and control are intimately linked.

APEX Attitude Simulation
 Case 9 $T_c=0.80$ $T_s=0.20$
 $Bi=500$, $Br=0$, $P=3$ s

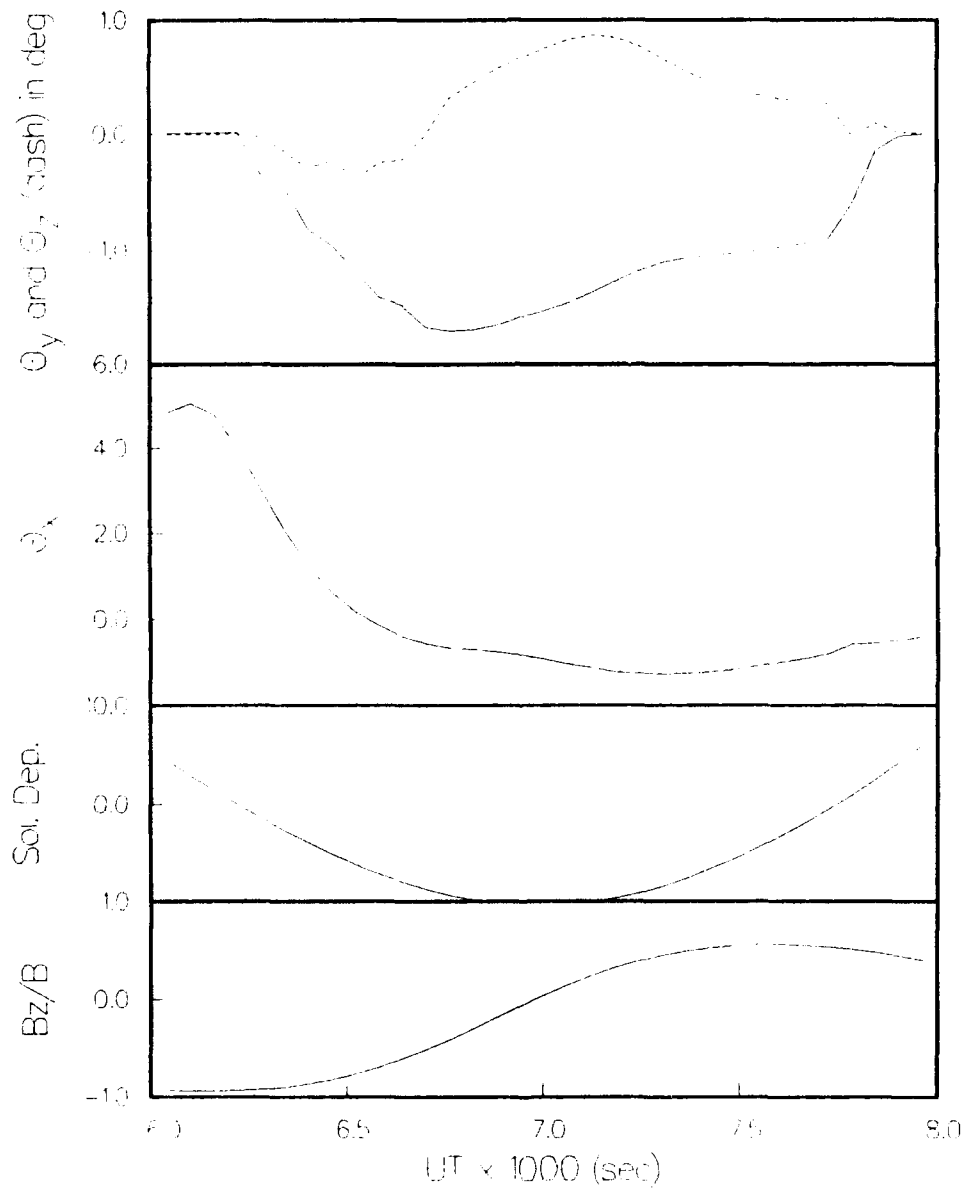


Figure 15. Pitch, yaw and roll angles during an eclipse.

Another thing to consider is that the complexity of the model $g(x)$ is generally inversely proportional to the difficulty in obtaining convergence. In the present application, a simple model that achieves reasonable accuracy with relative ease is preferable to a more complicated one of higher accuracy but which is more sensitive to initial guess and requires more careful convergence, since the adopted method may have to be run repeatedly in batch mode. A recalcitrant model could easily bog down the data processing. The model presented here has been designed with these considerations in mind.

In the simplest possible approach, we can approximate the attitude as a constant over some interval. The attitude is modeled in ECI coordinates by the right ascension α and declination δ of the spacecraft x-axis and by a phase ϕ of rotation around this axis. One representation of the attitude is [McNeil and Singer, 1986]

$$A = \begin{bmatrix} \cos\alpha\cos\delta & \sin\alpha\cos\delta & \sin\delta \\ \sin\delta\cos\alpha\sin\phi + \sin\alpha\cos\phi & \sin\delta\sin\alpha\sin\phi - \cos\alpha\cos\phi & -\cos\delta\sin\phi \\ \sin\delta\cos\alpha\cos\phi - \sin\alpha\sin\phi & \sin\delta\sin\alpha\cos\phi + \cos\alpha\sin\phi & -\cos\delta\cos\phi \end{bmatrix} \quad (51)$$

This parameterization has been chosen so that the nominal values of the attitude correspond to $\alpha = \alpha_s$ and $\delta = \delta_s$, the right ascension and declination of the sun, $\phi = 0$ in configuration 1 and $\phi = 180^\circ$ in configuration 2. The function to be minimized is taken to be

$$J = \sum_i (m_{x,i} - x \cdot b_i)^2 + \sum_i (m_{y,i} - y \cdot b_i)^2 + \sum_i (m_{z,i} - z \cdot b_i)^2 \quad (52)$$

where m_i is the i 'th component of the measured magnetic field and b_i the i 'th component of the field in inertial coordinates. The function is minimized by finding the zeros of the three simultaneous equations, the first of which is

$$\begin{aligned} F_\alpha = -\frac{dJ}{d\alpha} = & \sum_i (m_{x,i} - b_{x,i}C_\alpha C_\delta - b_{y,i}S_\alpha C_\delta - b_{z,i}S_\delta)(b_{x,i}S_\alpha C_\delta - b_{y,i}C_\alpha C_\delta) \\ & + \sum_i (m_{y,i} - b_{x,i}C_\alpha S_\delta S_\phi - b_{x,i}S_\alpha C_\phi - b_{y,i}S_\alpha S_\delta S_\phi + b_{y,i}C_\alpha C_\phi + b_{z,i}C_\delta S_\phi) \times \\ & (b_{x,i}S_\alpha S_\delta S_\phi - b_{x,i}C_\alpha C_\phi - b_{y,i}C_\alpha S_\delta S_\phi - b_{y,i}S_\alpha C_\phi) \\ & + \sum_i (m_{z,i} - b_{x,i}C_\alpha S_\delta C_\phi - b_{x,i}S_\alpha S_\phi - b_{y,i}S_\alpha S_\delta C_\phi - b_{y,i}C_\alpha S_\phi + b_{z,i}C_\delta C_\phi) \times \\ & (b_{x,i}S_\alpha S_\delta C_\phi + b_{x,i}C_\alpha S_\phi - b_{y,i}C_\alpha S_\delta C_\phi + b_{y,i}S_\alpha S_\phi) \end{aligned} \quad (53)$$

Where C stands for cosine and S for sine. The other two equations, F_δ and F_ϕ are obtained in the same way by differentiation of Eq(52) with respect to the appropriate variable. In the algorithm, the solution is found by a Newton-Raphson search technique, using numerical derivatives of the F_i . As a first guess, we assume that the spacecraft x-axis points at the sun and that the phase angle is zero. This calculation is carried out in a moving window, with the attitude at the midpoint assigned the value of the result of the calculation at that window. In order to include points at the beginning and end of the eclipse as midpoints of a window, we simply start a few minutes before and end a few minutes after the eclipse.

In the following paragraphs, we explore the behavior of this solution in the various situations of the test cases. In the first example, we assume, a 'random' field of 120 nT to test the response of the solution to noise. After that, we set the 'random' field to zero to better assess the characteristics of the solution without this complication. The static field is taken to be 500 nT and results of calibration of the magnetometer, discussed earlier, are used in all calculations. As we recall, 500 nT is probably somewhat excessive and constitutes therefore a 'worst case' insofar as the deviations of satellite operation from nominal.

In Figure 16 we show the solution for the eclipse presented in the previous figure. In one sense, at first glance, it is somewhat disappointing that we see errors of a degree or so in quantities, pitch, yaw, and roll, that are themselves only a few degrees in magnitude. However, we should consider these results in light of the inherent difficulty of specifying a changing attitude through the use of a set of single vector measurements. This is never a very happy situation. When the attitude changes, the best solution may not be the average attitude throughout the window. We have selected a seven minute window for Figure 16. Reducing the window would allow for a somewhat better result, but would also increase the noise level due to the random fields. With a three parameter model, we can use as few as three points. The actual choice in practice will depend to some extent on the noise level of the instrument. In any case, we can certainly conclude from Figure 16 that the satellite is operating normally, which is the main issue.

The solution is in error in proportion to the rapidity with which the attitude changes within a window. If the satellite remains within specified operating range, these changes will be small as in Figure 16 and the solution obtained will reflect proper operation, with errors of a degree or two. It is also approximately the same as that expected from the 100 nT or so 'random' induced fields. Improvements to the results of Figure 16 do not come easily. Adding parameters for time varying attitude requires increase in the window size for convergence and uniqueness. This in turn simply means that the attitude changes more within the window, giving results that are not substantially better. We have opted to stick with a constant parameterization and a relatively short window. In the following, we investigate the associated errors in several situations.

An interesting situation that is in some ways 'worst case' occurs in the second eclipse of Case 10. The attitude and the solution provided by the above algorithm are shown in Figure 17. We have chosen a three minute window for this calculation, which would be desirable whenever changes in attitude are greater than the instrument noise level. The effect is concentrated in the roll axis (θ_x) which can be seen to change rapidly at around 10,300 seconds UT. The reason is as follows. At that time, the magnetic field vector becomes nearly parallel to the spacecraft x-axis. This means that the spacecraft induced fields create a disproportionate angular error in the calculated roll. Even though the inclusion of induced fields in this simulation is somewhat artificial, there seems to be no reason why this effect should not be observed in practice to some extent. As the error increases, first in a positive sense then inflecting to the negative side, the satellite compensates for the erroneous calculated roll. Compensation and hence attitude change in the roll is rapid since the momentum wheel can act somewhat more efficiently than can the torque rods. Thus this effect would not be observed to so great an extent when the magnetic

APEX Eclipse, constant w/ 7 pts.
Case 9 Eclipse # 2

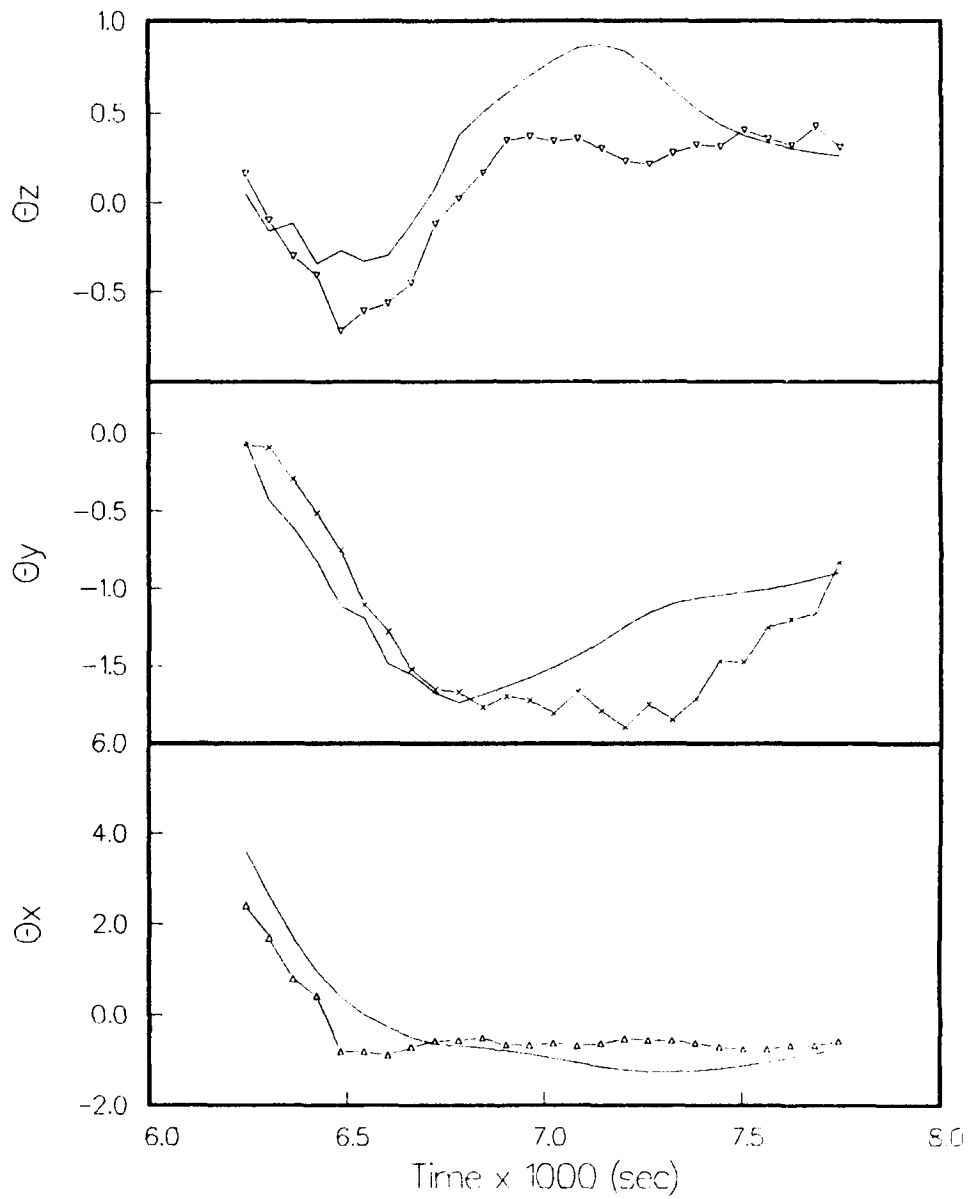


Figure 16. Best fit constant attitude solution with 7 points/fit.

APEX Eclipse, constant w/ 3 pts.
Case 10 Eclipse # 2

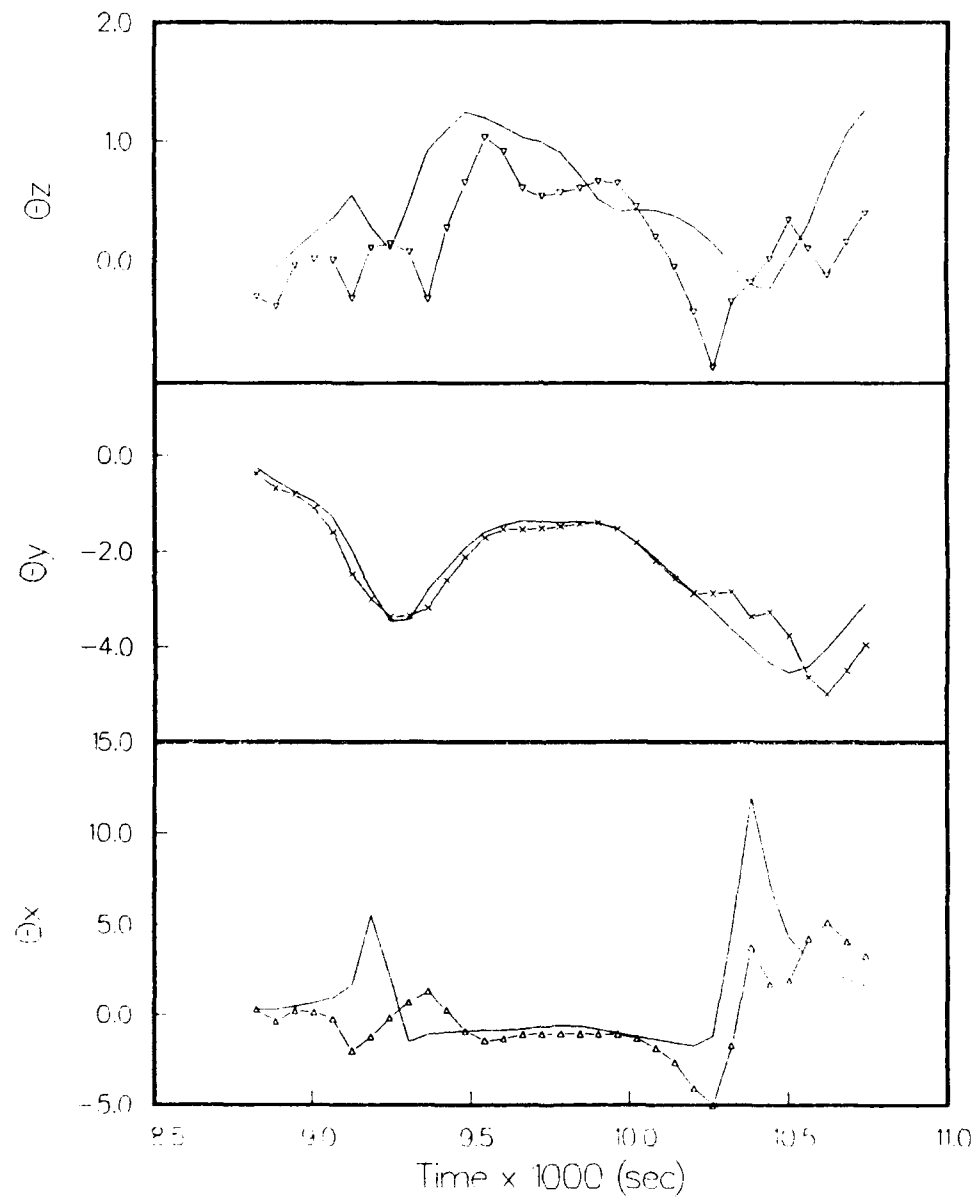


Figure 17. Attitude and solution (dots) for Eclipse 2 of Case 10.

field is perpendicular to the spacecraft x-axis instead. Although the solution has pretty much missed the rapid roll change, it at least reflects some aberrant behavior in roll.

Although this case gives rise to a rather large angular error in the calculated attitude, it too must be considered in light of the possibilities at hand. We believe that there is virtually no way to do substantially better when the attitude changes by 10° or so in the course of a few minutes. At least the solution has produced an attitude that is within a couple of degrees of correct for the x-axis (θ_y and θ_z) and has given us something near the average for the roll. This brings up another feature of the parameterization worth mentioning. The values of α and δ are determined primarily from the measurement of the spacecraft x-axis magnetic field. Had we solved using only these two parameters, that is,

$$J = \sum_i (m_{x,i} - (x \cdot b_i))^2 \quad (54)$$

we would have obtained almost identical results to those in Figure 17. This is nice in that there may well be motion in roll that is not echoed in pitch and yaw, and *vice versa*.

We should also test the solution algorithm on some very anomalous cases, since one of the major objectives of post-flight attitude determination is to verify nominal operation. One way to simulate non-nominal behavior is to increase the value of the static induced field B_i . In Figure 18, we show an eclipse for which $B_i = 2000$ nT. Again, since changes in attitude are large, we have used a short window. In this case, the roll and θ_y both exceed the 5° nominal limit. Although the rapid changes in roll cause the roll axis to be calculated with errors of up to about 5° , we see again that the error does not propagate strongly into the pitch and yaw calculations, where errors are nearer 2° . More importantly, the fact that the attitude exceeds the nominal limits in this case is evident from the calculated results. The last four points are, as usual, in substantially larger error due to the fact that they require post-eclipse points for their calculation. The pitch and yaw change rapidly after eclipse, recovering the sun within about four minutes.

As another test of the method in extremes, we look at the attitude that results from abandoning all attempts at control during eclipse. One such eclipse and the resulting solution is shown in Figure 19. We see that the pitch and yaw are relatively constant throughout and the roll error increases about linearly as the momentum wheel transfers the spin of the pitch and yaw axes to the roll axis. Although this is probably not an actual operational possibility, it is similar to the so called 'safe-hold' mode that will go into operation as a result of numerous anomalous conditions. In this mode, the roll axis is not controlled at all and will drift as in Figure 19. Pitch and yaw are controlled through torque rod operation and should remain small. We see in Figure 19 that the rapid change in roll (or ϕ) leads to errors of about 2° in the pitch and yaw determinations.

When in safe-hold mode, or at any other time when variation in roll greatly exceeds variation in pitch and yaw, there is a simple way to increase the accuracy of these solutions. If we let the variable $\phi(t)$ be parameterized by a constant and a linear term,

APEX Eclipse, constant w/ 3 pts.
Case 10 Eclipse # 3 BI=2000 γ

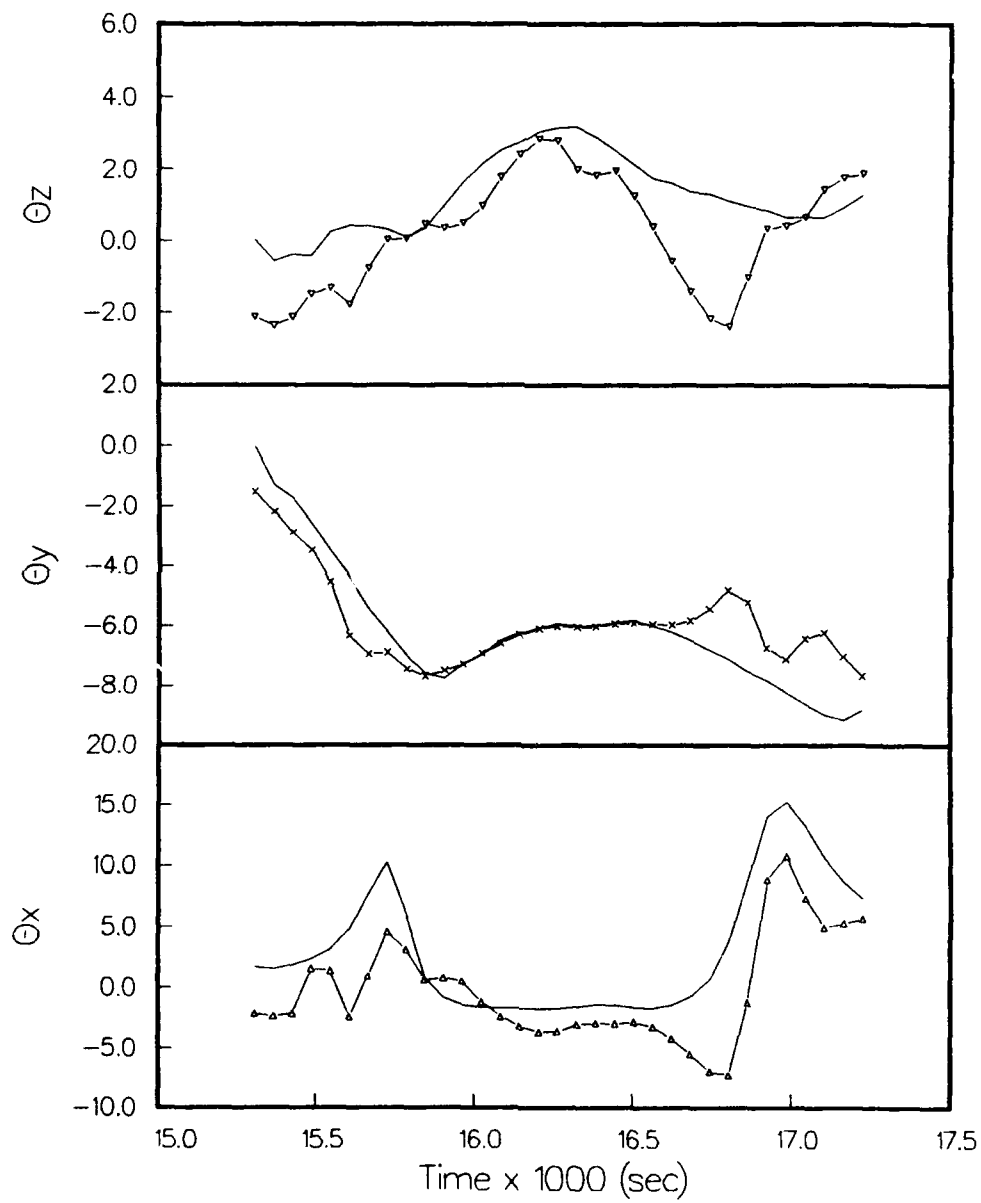


Figure 18. Attitude and solution (symbols) for a non-nominal case.

APEX Eclipse, constant w/ 7 pts.
Case 8 Eclipse # 8

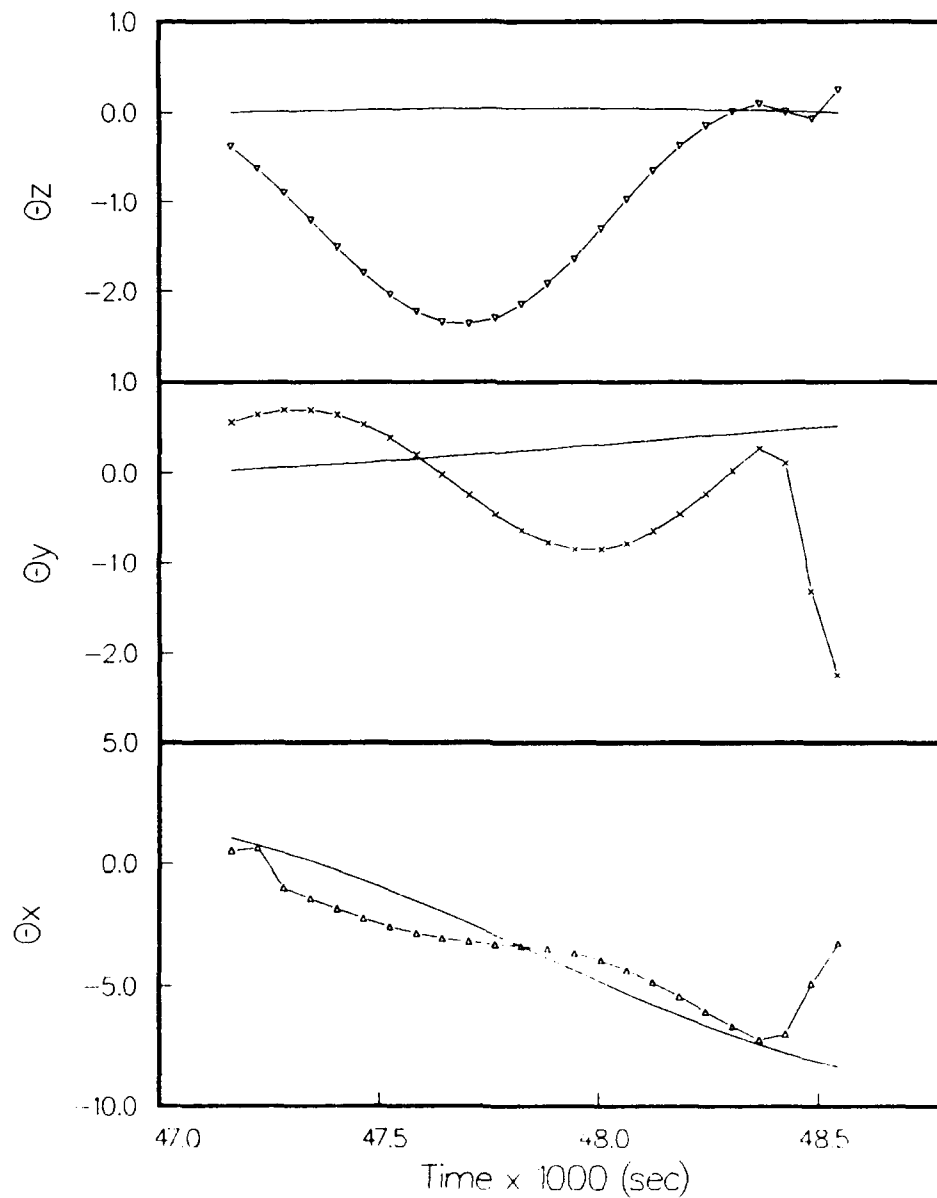


Figure 19. Attitude and constant solution for no control during eclipse.

$$\phi(t) = \phi_0 + \phi_1 t \quad (55)$$

and minimize with respect to the four variable parameterization, we obtain the results in Figure 20. Due to the clean separation of ϕ from α and δ in the problem, this set is also quite easy to minimize without convergence problems. As can be seen, the solution is quite good, until the final few points which suffer from the rapid reacquisition of nominal attitude immediately after eclipse. We will include this option in the solution package for use in safe-hold mode. Since changes in roll under normal operating conditions are often no more than those in pitch and yaw, use of this method there would probably not result in substantial improvement.

In summary, it appears that this method is capable of producing results accurate to around 2-3° when the attitude stays within nominal operational constraints. The method will thus be adequate for verification of nominal operation. Should the attitude stray greatly from nominal during eclipse, the error inherent in the calculation also will increase, at least with larger rates of change of the attitude parameters. However, the resulting attitude appears to be of adequate quality to judge the approximate degree of deviation from nominal. Errors are approximately the magnitude of the change in any attitude parameters within the window. In safe-hold mode, the addition of a linear term in roll removes the error due to rapidly changing roll. These algorithms appear as the methods of choice, since they are adequate for control assessment, do not require initial values and are rapidly convergent.

5.0 EVALUATION OF ON-BOARD ATTITUDE

In addition to the verification of nominal operations, we must decide in the course of attitude processing whether the post-flight or the on-board attitude best represents the actual attitude. Discretionally, either one or the other will be included on Agency Tapes for the perusal of experimenters. During sunlight operations, this decision presents no great problem since, barring magnetometer calibration problems, the two solutions should be identical. The decision then shifts to one of which set of calibration factors are the best. This can be evaluated independently by comparison with model fields.

In eclipse, we are faced with a more difficult problem. What, for example, if we plotted the on-board and post-flight solutions and came up with something like Figure 16, with agreement to about 2-3°? There is a way by which we can at least verify the self-consistency of the on-board solution. Accompanying the on-board pitch, yaw and roll data will be rates of change of pitch, yaw and roll. We can use these to approximate the rates of change in α , δ and ϕ and thereby greatly increase the level of accuracy of our parameterization. These rates of change are given by

APEX Eclipse, w/ $d\phi/dt$ & 7 pts.
Case 8 Eclipse # 8

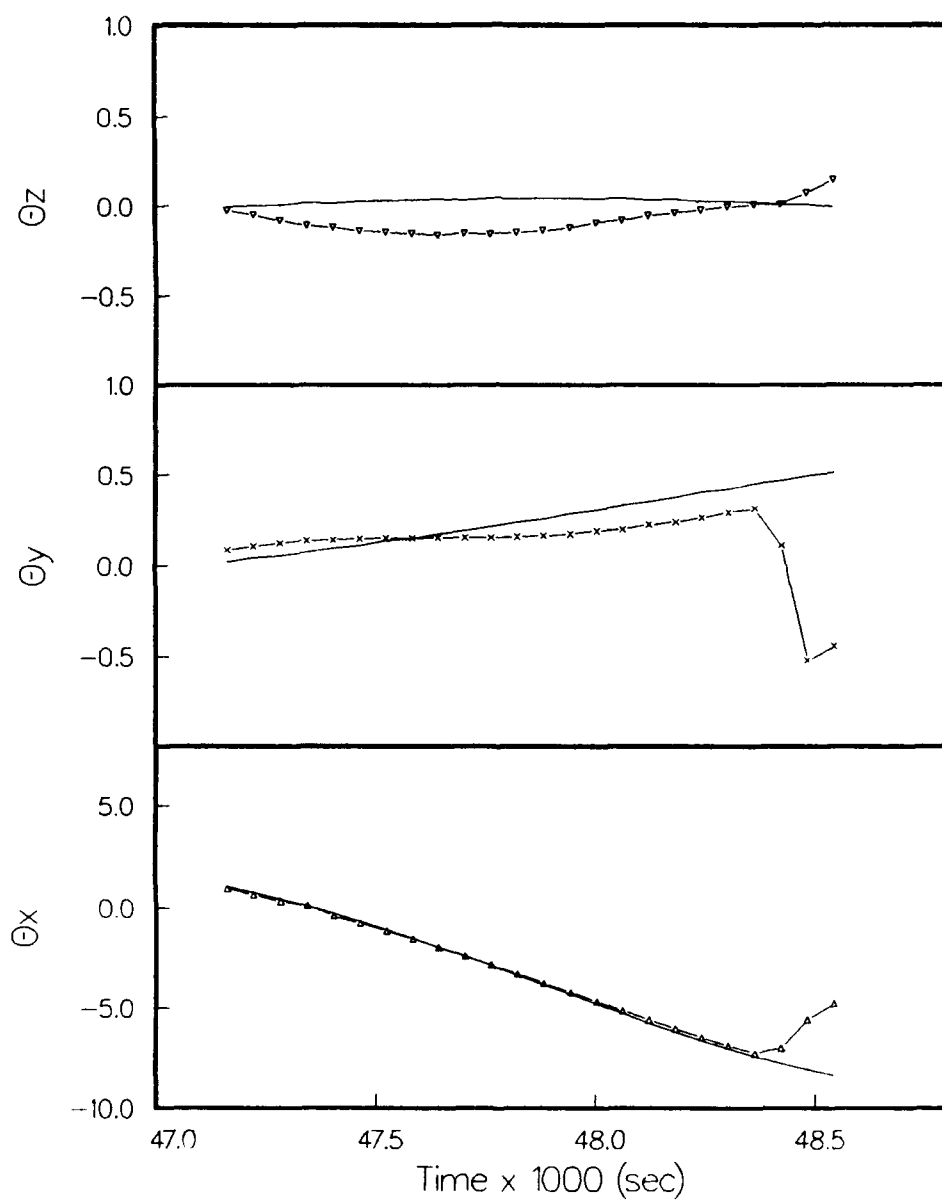


Figure 20. Same as Figure 19 but with a linear term in ϕ .

$$\frac{d\alpha}{dt} \approx -\frac{d\theta_z}{dt} \quad \frac{d\delta}{dt} \approx \frac{d\theta_y}{dt} \quad \frac{d\phi}{dt} \approx \frac{d\theta_x}{dt} \quad (56)$$

In the eclipse algorithm, we minimize $\alpha_0 + \alpha_1 t$, etc. where α_1 remains fixed at the reported rate of change given in telemetry. Should this give rise to a solution more like the on-board solution, assuming that both solutions are comparable, we would be inclined to elect the on-board solution for Agency Tape generation. Figure 21 repeats the eclipse of Figure 16 but with fixed derivatives obtained from the attitude simulation. Should the on-board and post-flight attitude come out markedly different, however, the self-consistency of the on-board attitude and rates is not a sufficient indication of the better quality of the on-board solution.

6.0 CONCLUSION

We have modeled the APEX ephemeris and attitude over the course of several days, encompassing a variety of situations and have observed the response of the satellite using realistic environmental and control torques. Using these results, algorithms have been developed and tested for magnetometer calibration and for attitude solution. Although the results of this model may well be substantially different from the actual attitude behavior, we believe that the relative success of the computations on simulated data will be reflected in the experience with real data. The verification of the sun to solar panel angle during sunlit operations is straightforward and should be accurate to a few tenths of a degree. It appears to be possible to calculate the roll angle in sunlight and the three attitude angles during eclipse to a precision of perhaps a factor of two higher than the nominal allowed deviations of 5° in the attitude. Although, for verification purposes, a larger margin would be preferable, the present situation allows for the determination of attitude control with reasonable confidence.

In closing, we should reiterate the importance of this type of simulation in the development of attitude determination software. Although it may appear somewhat overly complicated and even repetitive, since OSC has also performed these types of simulations, it is altogether necessary. Without simulation of the environmental torques along with the restoring torques commanded by the actual control laws, we would be left with considerable uncertainty in the definition of the attitude itself. Without simulation, too, we would have no indication of the degree or rate of attitude change during eclipse, and thus would not be able to evaluate the effectiveness of the chosen solution algorithm. Assuming a constant attitude, for example, would have led to a result in precise agreement with the attitude. We have seen, however, that errors in practice may be substantially larger, but still tolerable. The fact that we have tested the proposed algorithms, along with the general familiarity with the expected attitude and sensor data conferred by simulation, gives us considerably more confidence of successful and expedient evaluation of the actual attitude data, once it is in hand.

APEX Eclipse, w/ deravitives 7 pts.
Case 9 Eclipse # 2

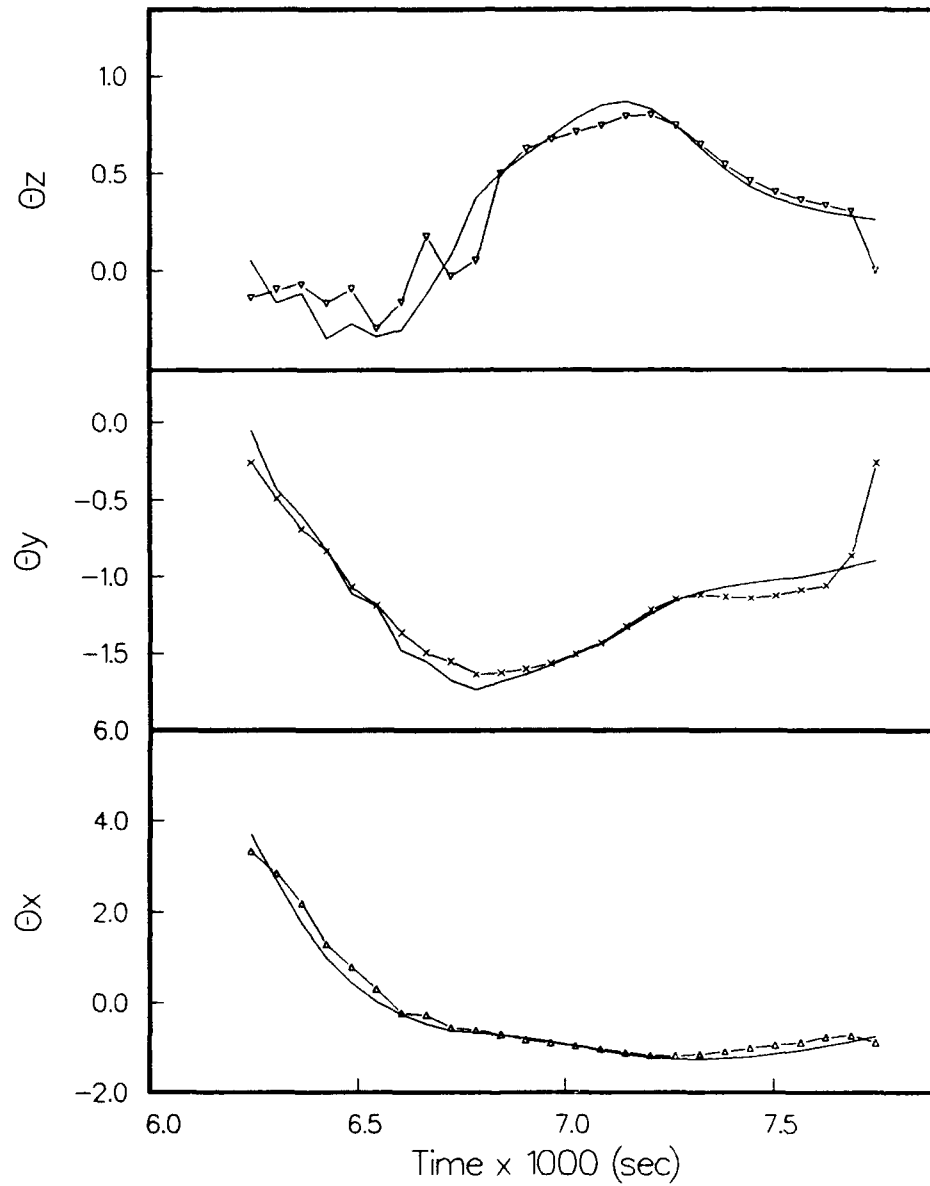


Figure 21. Case 9 Eclipse 2 solution, calculated with 'known' rates of change.

REFERENCES

- Ball Aerospace, "Verification Test Report for Alignment Measurements of CRRES", CRRES-915, Ball Space Systems Division, Boulder, Co., 9 March 1990.
- Barnison, R., *private communication*, 1992.
- Kwok, J. H., "The Artificial Satellite Analysis Program (ASAP)", Jet Propulsion Laboratory, Pasadena, Calif., April 1987.
- McNeil, W. and H. J. Singer, "Fluxgate Magnetometer Analysis and Simulation Software for CRRES", AFGL-TR-86-0222, 1 October 1986, ADA176353.
- McNeil, W., "Software Detailed Design Document for the APEX Orbital Data Processing System Ephemeris Computation Function", Radex, Inc., Bedford, Mass. (APEX-EPH-02) 20 April 1992.
- Orbital Sciences Corp., "APEX ACS Code Walkthrough", Fairfax, Va., 30 April 1992.
- Space Sciences Corp., *private communication*, 1991.
- Stoltz, P., "APEX Critical Design Review: Attitude Determination and Control Subsystem", Fairfax, Va., 5-8 November 1991.
- Wertz, J. R., ed., "Spacecraft Attitude Determination and Control", D. Reidel Publishing Company, Boston, 1986.

Appendix - State Vectors

The following state vectors were used to generate the ephemeris for this study. The coordinate system is true-of-date Earth Centered Inertial.

X(km)	Year	Day	Second	Rev #	Vx(km/s)	Vy(km/s)	Vz(km/s)
			Y(km)	Z(km)			
5922.681152	91	0	0.000	1 0.0000			
			-2312.936035	2227.808838	3.38994217	1.82176983	-7.11462641
333.102753	91	1	0.000	14 0.0000			
			2673.440674	-7309.891602	-6.71503830	2.03565097	-0.30837882
-7843.144043	91	2	0.000	27 0.0000			
			2569.690186	-104.129593	-0.50028402	-2.21145177	6.20766211
-34.582718	91	3	0.000	41 0.0000			
			-2538.974121	6590.689941	7.30961275	-2.06632018	-1.46704304
5658.311035	91	4	0.000	54 0.0000			
			-571.851929	-4303.395020	-3.25924301	3.62198353	-5.92411470
-4664.481445	91	5	0.000	67 0.0000			
			4196.505859	-5401.880859	-4.96536970	0.47305381	4.29641962
-5845.307617	91	6	0.000	81 0.0000			
			798.506714	4966.917480	4.15876436	-3.75541592	4.36136055
5229.038086	91	7	0.000	94 0.0000			
			-3639.860840	2209.513184	3.78598666	0.92756629	-7.07966566
1119.718994	91	8	0.000	107 0.0000			
			2464.516357	-7403.245117	-5.94886065	3.54509449	-0.41860914
-6939.483398	91	9	0.000	120 0.0000			
			4365.214844	-279.218292	-1.07204473	-2.01031303	6.25145912
-394.175568	91	10	0.000	134 0.0000			
			-2558.539063	6460.285645	6.71218014	-3.69477177	-1.67764628
5339.558594	91	11	0.000	147 0.0000			
			-1731.985596	-4604.779297	-2.48622346	4.29536104	-5.67568588